공학석사학위논문

Numerics Applied Nanofluid Analysis in a Square Array Subchannel

사각 배열 부수로에서의 나노유체 적용에 대한 수치해석

2015 년 8 월

서울대학교 대학원

원 자 핵 공 학 과

Shamim Jubair Ahmed

Numerics Applied Nanofluid Analysis in a Square Array Subchannel

사각 배열 부수로에서의 나노유체 적용에 대한 수치해석

지도 교수 서 균 렬

이논문을 공학석사학위논문으로 제출함

2015 년 7 월

서울대학교 대학원

원 자 핵 공 학 과

주 바 이 르

주바이르의 석사학위 논문을 인준함

2015 년 7 월

위 원 장 김 응 수 (인)

부위원장 서 균 렬 (인)

위 원 조 형 규 (인)

Abstract

Numerics Applied Nanofluid Analysis in a Square Array Subchannel

Shamim Jubair Ahmed

Department of Nuclear Engineering

School of Energy Systems Engineering

Seoul National University

This dissertation treats the thermohydrodynamic performance of alumina (Al_2O_3) nanofluid in a square array subchannel featuring pitch-to diameter (*P/D*) ratio of 1.25 and 1.35 to check its applicability in a typical Pressurized Water Reactor (PWR) rod bundle under single phase turbulent flow condition. Two fundamental aspects of thermal hydraulics viz. augmentation of convective heat transfer coefficient and accompanied pressure drop have been discussed using pure water and different volume concentrations (0.5%, 1.5% and 3.0%) of water/alumina (Al_2O_3) nanofluids as coolant.

A widely used and commercially available CFD package "STAR-CCM+ (ver. 9.06.011)" has been utilized to carry out numerical simulation by setting up flow as single phase, incompressible and turbulent for different inlet Reynolds number, *Re* spanning from 3×10^5 to 6×10^5. The realizable k-ε model is implemented to simulate turbulence inside subchannel. Despite the results of a simulation performed in a single subchannel may not be reliable

for analyzing the entire rod bundle, however, their quantitative and qualitative similarity can readily be utilized as a preliminary step in fixing thermohydrodynamic parameters of a rod bundle.

The numerical results revealed that convective heat transfer coefficient, h (W/m^2.K) is augmented with increasing nanoparticle volume concentration in the subchannel geometry. While for the same inlet *Re*, maximum heat transfer increment of about 22% is achieved for 3.0% particle volume concentration of alumina nanofluid, using same mass flow rate at inlet boundary and for same vol.% it is observed that convective heat transfer coefficient of nanofluid is slightly lower compared to pure water.

The pressure drop is found to be increased significantly with the augmentation of particle volume concentration of alumina nanofluid due to increased viscosity and density and in case of 3.0% volume concentration pressure drop increment is about 56% compared to that of pure water.

Finally, a multiple regression analysis has been performed to propose a new correction factor for an existing correlation of square array subchannel to obtain Nusselt number, *Nu* more accurately for nanofluids in such geometry.

Keywords:

Subchannel Analysis, Numerical Simulation, PWR Type Reactor, Heat Transfer, Pressure Drop, Alumina Nanofluid

Student Number: 2013-23865

Contents

List of Tables

List of Figures

Acronyms

BWR	Boiling Water Reactors
CFD	Computational Fluid Dynamics
CHF	Critical Heat Flux
ECCS	Emergency Core Cooling System
HCl	Hydrochloric Acid
HTC	Heat Transfer Coefficient
LWR	Light Water Reactors
LB-LOCA	Large Break- Loss of Coolant Accident
MIT	Massachusetts Institute of Technology
MWe	Megawatt Electricity
NUIDEA	Nuclear Units Informatics Design Engineering Architect
PCT	Peak Cladding Temperature
PWR	Pressurized Water Reactors

Chapter 1. Introduction

“Nanotech + Nuclear = More Electricity”

Efficient engineered design of heat transfer and fluid flow (conjugately termed as thermo-hydrodynamics) with enhanced heating or cooling are two pivotal aspects that must be taken into consideration while converting nuclear energy into thermal energy by extraction of heat from the nuclear fuel elements in order to save energy, reduce process time, raise thermal rating and increase the working life of reactor pressure vessel. Hence, a major challenge in designing a new nuclear power plant is the quantification of the optimal flow of coolant and distribution of pressure drop across the reactor core. While higher coolant flow rates will lead to better heat transfer coefficients and higher CHF limits, it will also result in larger pressure drops across the core, therefore larger demand of pumping powers as well as larger dynamic loads on the core components. Thus, the role of the hydrodynamic and thermal-hydraulic core analysis is to find proper working conditions with enhanced heat transfer and reduced pressure drop that will assure both safe and economical operation of the nuclear power plants.

In the recent era, nanofluid has gained much attention as a promising coolant for PWR rod bundle due to its enhanced thermal capabilities with insignificant rise in pressure drop. While most conventional designs to elevate heat transfer performance are limited to only variation of mechanical structures, such as addition of heat surface area (fins), vibration of heated surface, injection

or suction of fluids, applying electrical or magnetic fields etc., application of these techniques in a nuclear fuel rod assembly will require not only designing complex core geometries but also elevate the manufacturing cost as well as may jeopardize essential safety features accompanied by reduced lifetime of reactor pressure vessel. Hence, nanofluid coolant with its tiny particle size, relatively large surface area and small volume fraction can be an outstanding alternatives for PWR coolants.

Recently a group of researchers led by Professor Jacopo Buongiorno and Dr. Lin-wen Hu from MIT has wetted the appetite of using nanofluid coolant in PWR by demonstrating a recipe for getting 20 percent more electricity out of today's nuclear power plants. The key ingredient is just sprinkling of tiny nanoparticles added to the PWR coolant and thus removing more heat from hot nuclear fuel to power conversion equipment. Their research has revealed that using the nanofluid rather than the pure water can raise the heat-removal limit by as much as 70 percent. Calculations based on that finding suggest that replacing the water coolant with the nanofluid in a 1000-megawatt-electric (MWe) nuclear plant could push the plant's output up to 1200 MWe. Last but not least, the necessary concentration of particles is low-just 0.1 percent by volume or less. "So it's like a magic powder," said Buongiorno. "You put a tiny bit in and you get this spectacular effect."

Apart from PWR main coolant, other potential applications of nanofluid in a nuclear power plant may include but not limited to using it as coolant for emergency core cooling system (ECCS) of both PWRs and BWRs and coolant

for in-vessel retention of the molten core at the time of severe accidents in high-power density LWRs [1].

Despite nanofluid is capable of augmenting the heat transfer capability remarkably, clustering phenomenon of nanoparticles may eventually decrease the thermal conductivity and initiate problems like corrosion and wear inside piping and pumps. Hence, more research initiatives are necessary in this area to propose a satisfactory explanation for preventing clustering in nanoparticles suspensions.

The purview of this dissertation is limited to investigation of thermal-hydraulic performance of water/ alumina (Al_2O_3) nanofluid in terms of heat transfer and pressure drop in a square array subchannel. In this regard, a numerical simulation has been carried out by using a commercial CFD tool "STAR-CCM+ (ver. 9.06.011)." The organization of this dissertation is ramified into five chapters as follows:

Chapter 1 introduces the research background and motivation for prioritization of numerical modeling, review of state-of-the-art on convective heat transfer enhancement of nanofluid and CFD simulation of rod bundles to evaluate heat transfer and pressure drop characteristics.

Chapter 2 cracks the thermophysical properties as well as heat transfer enhancement mechanism of nanofluid, effect of surface deposition on critical heat flux and convective heat transfer coefficient enhancement of nanofluid, chemical and physical stability of nanofluid under irradiation.

Chapter 3 initiates the compendium of CFD methodology which includes but not limited to governing equations of CFD, elements of a CFD code, properties of good numerical solution and a brief introduction of STAR-CCM+ which is a commercial CFD code developed by CD-Adapco with a view to introduce an user friendly engineering tool not only limited to experts within the CFD arena.

Chapter 4 treats the detailed procedure of numerical methodology for simulating heat transfer and pressure drop in a square array subchannel with pure water and different volume concentrations of water/ alumina (Al_2O_3) nanofluid using STAR-CCM+.

Chapter 5 provides the detailed information on model validation for the present study, summary of numerical outcome for heat transfer and pressure drop, quantitative and qualitative comparison of numerical data with well-known correlations available in literature and last but not least, development of new correction factor for the square array subchannel to predict Nusselt number as well as convective heat transfer more precisely.

Finally, instrumental findings of the present study have been summarized under conclusion.

1.1Background and Motivation

"Nanotechnology: It's a Small, Small, Small, Small World"

(Dr. Ralph C. Merkle)

It's really hard to envision just how small nanotechnology is. According to the International System (SI) of Units, the prefix "nano" refers to one-billionth, or 10^{-9}; hence one nanometer equals to one-billionth of a meter. It's hard to imagine just how small that is, so here are some paradigms given below:

- A sheet of paper is about 100,000 nanometers thick.
- A strand of human DNA is 2.5 nanometers in diameter.
- A human hair is approximately 80,000- 100,000 nanometers wide.
- On a comparative scale, if the diameter of a marble was one nanometer, then diameter of the Earth would be about one meter.

A pictorial description of the scale of nanotechnology, depicting how small things at the nanoscale actually are is presented in Fig. 1.1:

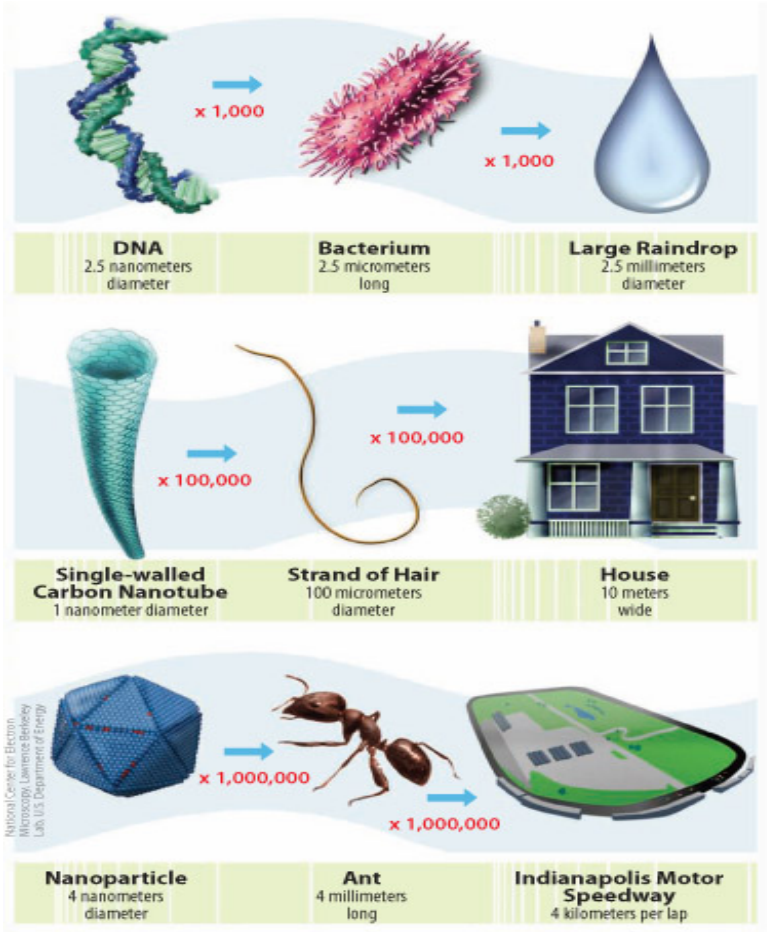

Fig. 1.1: The scale of nanotechnology

(Source: http://www.nano.gov/nanotech-101/what/nano-size)

Despite engineers have been working for decades to develop more efficient heat transfer fluids for industrial applications, until recent times they could only create microparticles- large enough even to be visible by naked eyes accompanying a diameter thousand times greater than nanoparticles. These microparticles were so large in size that they would likely to settle out rapidly and precipitated at the bottom of a tank or pipe. Even if the fluid was kept stirring continuously, the microparticles would damage the walls of pipe,

wearing them thin. The abrasive particles would also tend to wear out pumps and bearings so quickly.

But the dramatic advancement of modern science has made it possible to beget ultrafine particles of nanosized diameter, and thus has made a breakthrough in solving the long lasting heat transfer enhancement problem in different industry. In fact, these particles are so small that in some cases, that there is little or no settling of the particles after even months.

Therefore, nanofluid is being considered as a promising coolant for existing light water nuclear reactors to enhance heat transfer capability as well as uprate core power density in the recent times. The improved heat transfer performance of nanofluids is due to the fact that the nanoparticles:

- Increase the surface area and heat capacity of the fluid.
- Improve the thermal conductivity of the fluid.
- Cause more collisions and interactions between the fluid, particles and flow passages.
- Cause more turbulence and mixing of the fluid.

1.2 Nuclear Applications of Nanofluid

Boungiorno et al. [1] at the Massachusetts Institute of Technology (MIT) have carried out exhaustive research on nanofluid heat transfer for PWR applications that encompassed but not limited to pool-boiling heat transfer and CHF, as well as flow boiling CHF and summarized the potential applications as follows:

- Use of nanofluid as a primary coolant in PWRs to augment the core power density.
- Use of nanofluid in the accumulators and safety injection of emergency core cooling systems (ECCS) to elevate design-basis accident tolerance.
- Use of nanofluid for flooding of reactor cavity to increase safety limit during severe accidents.

1.2.1 PWR Main Coolant Application

Water based nanofluids have been considered as a promising coolant for existing and/or future PWRs as an effective means of making them economically more alluring. Experiments as well as analytical studies have shown that use of nanofluid with at least 32% higher CHF is capable to enhance a 20% power density in current nuclear power plants without altering the fuel assembly design and without reducing margin to CHF [1]. One major problem in using nanofluid coolant lies in is its higher viscosity at loadings greater than 1.0 vol.% which is not acceptable in nuclear systems. However, Boungiorno et al. have proved that CHF gains are possible with low nanoparticle loadings at which the viscosity, thermal conductivity, surface tension and specific heat of water based nanofluid are very close to those of pure waters. Apart from that, they have also simulated a 17×17 PWR fuel assembly with a LWR neutronic code called CASMO and showed that use of nanofluid has negligible penalty on reactivity as well as void reactivity coefficient as depicted in Fig. 1.2 [2].

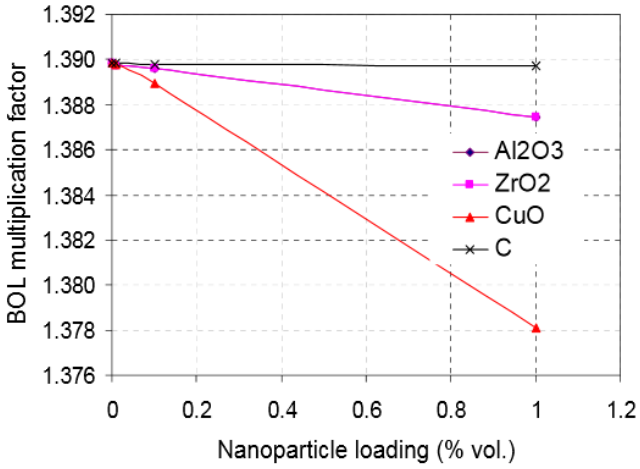

Fig. 1.2: Effects of nanoparticle loading on reactivity [2]

1.2.2 ECCS Application

Nanofluids can also be used in the Emergency Core Cooling Systems (ECCS) incorporated in both PWRs and BWRs during a LB-LOCA. During a LB-LOCA the peak cladding temperature (PCT) should be kept below 1200 ^{0}C to hinder rapid oxidation of the cladding materials for which a key factor is an increment in post-CHF heat transfer during reflood which can be easily achieved by use of nanofluid in ECCS water without having dramatic effect on blowdown [1].

1.2.3 Severe-Accident Application

Nanofluids are also being considered as potential coolants for in-vessel retention (IVR) of a molten core during a hypothetical severe accident scenario in high power density LWRs which involves flooding of the reactor cavity and removal of residual heat from the molten core through reactor vessel lower head. In this case, heat removal is subject to the occurance of CHF on the

reactor vessel outer surface, margin for which can readily be increase by using nanofluid instead of pure water for better mitigation of severe accidents. A typical nanofluid injection system proposed by MIT researchers has been shown in Fig. 1.3 [1].

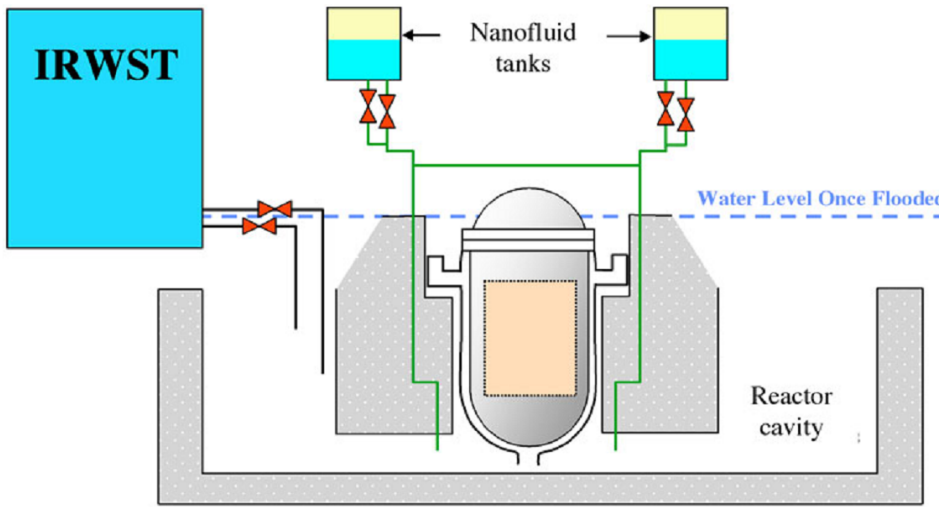

Fig. 1.3: Schematic of nanofluid injection systems for severe-accident management [1]

1.3 State of the Art on Convective Heat Transfer Enhancement by Nanofluid

In order to implement nanofluids as a coolant in nuclear power plants as well as to materialize their practical applications, it is first necessary to understand their convective heat transfer characteristics. Literature on connective heat transfer enhancement of nanofluids are supernumerary and hence the scope of discussion in this chapter will be limited to few remarkable works on forced convection of nanofluids in both turbulent and laminar region.

1.3.1 Experimental Studies

One notable experimentation was carried out by Pak & Cho [3] to observe the turbulent friction and heat transfer behaviors of dispersed fluids in a circular pipe using two different metallic oxide particles, γ-alumina (Al_2O_3) and titanium dioxide (TiO_2) with mean diameters of 13 and 27 nm, respectively. The results revealed that the Nusselt number for the dispersed fluids increased with increasing volume concentration as well as Reynolds number. But at constant average velocity, the convective heat transfer coefficient of the dispersed fluid was 12% smaller than that of pure water. They proposed a new correlation as presented by Eq. (1.1) for the Nusselt number under their experimental ranges of volume concentration (0-3%), the Reynolds number (10^4 - 10^5), and the Prandtl number (6.54 - 12.33) for the dispersed fluids γ-alumina (Al_2O_3) and titanium dioxide (TiO_2) particles as given below:

$$Nu_{nf} = 0.021 \mathrm{Re}_{nf}^{0.8} \mathrm{Pr}_{nf}^{0.5} \tag{1.1}$$

Xuan and Li [4] carried out experimentation to observe the flow and convective heat transfer feature of the Cu-water nanofluid flowing through a straight brass tube. of the inner diameter of 10 mm and the length of 800 mm. The results revealed that suspended nanoparticles are capable to enhance heat transfer process remarkably and at fixed velocities, the heat transfer coefficient of nanofluids containing 2.0 vol% Cu nanoparticles was improved by as much as 40% compared to that of water. The Dittus–Boelter correlation failed to predict this improved experimental heat transfer behavior of nanofluids. They have proposed a new correlation in the form of Eq. (1.2) to correlate the

experimental data for the nanofluid. The Nusselt number, *Nu* for the turbulent flow of nanofluids inside a tube can be obtained as follows:

$$Nu_{nf} = 0.0059\left(1.0 + 7.6286\varphi^{0.6886} Pe_P^{0.001}\right) \mathrm{Re}_{nf}^{0.9238}\ \mathrm{Pr}_{nf}^{0.4} \qquad (1.2)$$

Effect of particle size on the convective heat transfer in nanofluid at the developing region of pipe flow with constant heat flux was analyzed by Anoop et al. [5]. The results revealed that at *x/D* = 147, for 45 nm particle based nanofluid (4 wt%) with *Re* = 1550, the enhancement in heat transfer coefficient was around 25% whereas for the 150 nm particle based nanofluids it was found to be around 11%. After conducting sufficient number of experiments, they proposed the following correlation:

$$Nu_x = 4.36 + \left[a.x_+^{-b} \left(1 + \varphi^c\right).\exp^{(-d.x_+)} \right] \left[1 + e.\left(\frac{d_p}{d_{ref}} \right)^{-f} \right] \qquad (1.3)$$

where, a= 6.219×10^{-3}, b=1.1522, c=0.1533, d=2.5228, e=0.57825, f=0.2183, d_{ref}=100 nm, d_p=diameter of particle in nm, φ= volume fraction in percentage.

Chandrasekar et al. [6] carried out experiments to observe convective heat transfer and pressure drop characteristics of Al_2O_3/water nanofluid in the fully developed laminar region of pipe flow with constant heat flux with and without wire coil inserts. It was observed that dilute 0.1% Al_2O_3/water nanofluid increased the Nusselt number by 12.24% at *Re* = 2275 compared to that of distilled water. Further enhancements in Nusselt numbers was observed when Al_2O_3/water nanofluid is used with wire coil inserts. Nusselt numbers were increased by 15.91% and 21.53% when Al_2O_3/water nanofluid was used

with their two types of wire coil inserts respectively at *Re* = 2275 compared to those of distilled water. The Nusselt number and friction factor experimental results have been correlated in the form of Eq. (1.4) and Eq. (1.5) valid for laminar flow with *Re* < 2300, dilute Al_2O_3/water nanofluid with volume concentration φ = 0.1% and wire coil inserts with $2 \le P/D \le 3$:

$$Nu_{nf} = 0.279\left(\mathrm{Re.Pr}\right)_{nf}^{0.558}\left(\frac{P}{D}\right)^{-0.447}\left(1+\varphi\right)^{134.65} \tag{1.4}$$

$$f = 530.8\,\mathrm{Re}_{nf}^{-0.909}\left(\frac{P}{D}\right)^{-1.388}\left(1+\varphi\right)^{-512.26} \tag{1.5}$$

Suresh et al. [7] performed experiments on convective heat transfer and pressure drop characteristics of three different concentration of CuO/water nanofluid in the fully developed turbulent region of pipe flow with constant heat flux. Experiments were done with a dimpled tube having dimensions of 4.85 mm diameter and 800 mm length. They concluded that the convective heat transfer coefficient increases with increasing Reynolds number and increasing volume concentration in plain tube, and increases further with a dimpled tube. The experimental data for Nusselt number and friction factor of nanofluids with dimpled tubes have been correlated by the following expressions [Eq. (1.6) and Eq. (1.7)] using the least squares regression analysis:

$$Nu_{nf} = 0.00105\,\mathrm{Re}_{nf}^{0.984}\,\mathrm{Pr}_{nf}^{0.4}\left(1+\varphi\right)^{-80.78}\left(1+\frac{P}{D}\right)^{2.089} \tag{1.6}$$

$$f = 0.1648\,\mathrm{Re}^{0.97}\left(1+\varphi\right)^{107.89}\left(1+\frac{P}{D}\right)^{-4.463} \tag{1.7}$$

Hojjat et al. [8] experimentally investigated the forced convection heat transfer of non-Newtonian nanofluids in a circular tube with constant wall temperature under turbulent flow conditions using three types of nanofluids by dispersing homogeneously γ-Al_2O_3, TiO_2 and CuO nanoparticles into the carboxymethyl cellulose (CMC) as base fluid. The test section consists of two 2-m long concentric tubes made of stainless steel (type 316). Results indicated that the convective heat transfer coefficient of nanofluids is higher than that of the base fluid. The enhancement of the convective heat transfer coefficient increases with an increase in the Peclet number and the nanoparticle concentration. Experimental data were compared to heat transfer coefficients predicted using available correlations for purely viscous non-Newtonian fluids. Since, the results showed poor agreement between experimental and predicted values, they proposed a new correlation as presented by Eq. (1.8) to predict Nusselt numbers of non-Newtonian nanofluids more accurately valid for $2900 \leq Re \leq 8800$ and $39 \leq Pr \leq 71$:

$$Nu_{nf} = 0.00115\,\mathrm{Re}_{nf}^{1.05}\,\mathrm{Pr}_{nf}^{0.693}\left(1+\varphi^{0.388}\right) \tag{1.8}$$

1.3.2 Numerical Studies

One well cited work carried out by Maiga et al. [9] is the numerical study of fully developed turbulent flow of water/ Al_2O_3 nanofluid in circular tube having diameter of 0.01m and a total length of 1.0 m with a uniform heat flux of 50 W/cm^2. The classical k-ε model was used for turbulence modeling and the results clearly showed that the inclusion of nanoparticles into the base fluids has produced a considerable augmentation of the heat transfer coefficient

that clearly increases with an increase of the particle concentration. Two different mixtures studied, among which the ethylene glycol/ γ-Al_2O_3 nanofluid appears to offer a better heat transfer enhancement than water/ γ-Al_2O_3. The following correlations [Eq. (1.9) and Eq. (1.10)] have been proposed to evaluate the averaged Nusselt number for the nanofluids considered for both the thermal boundary conditions, valid for $Re \leq 1000$, $6 \leq Pr \leq 7.53$ and $\varphi \leq 10\%$:

For constant wall flux:

$$Nu_{nf} = 0.086\,\mathrm{Re}_{nf}^{0.55}\,\mathrm{Pr}_{nf}^{0.5} \tag{1.9}$$

For constant wall temperature:

$$Nu_{nf} = 0.28\,\mathrm{Re}_{nf}^{0.35}\,\mathrm{Pr}_{nf}^{0.36} \tag{1.10}$$

In another numerical study carried out by Maiga et al. [10] for turbulent flow in a tube using different concentrations of Al_2O_3 nanoparticle suspension under the constant heat flux boundary condition the following correlation [Eq. (1.11)] has been proposed to estimate the heat transfer coefficient in terms of the Reynolds and the Prandtl numbers, valid for $10^4 \leq Re \leq 5\text{x}10^5$, $6.6 \leq Pr \leq 13.9$ and $0 \leq \varphi \leq 10\%$:

$$Nu_{nf} = 0.085\,\mathrm{Re}_{nf}^{0.71}\,\mathrm{Pr}_{nf}^{0.35} \tag{1.11}$$

Bianco et al. [11] numerically modelled forced convection laminar flow of water/ Al_2O_3 nanofluid flowing through a circular tube subject to a constant and uniform heat flux. They analyzed both a single and two-phase model (discrete particle model) for particle size equal to 100 nm and for φ=1%

& 4%, *Re*=250, 500, 750 & 1050 and *q"*=5000, 7500 and 10,000 W/m^2. The results revealed that the difference between the results of single phase and two-phase approaches is small (approximately 11%), especially when temperature dependence of thermophysical properties is taken into account. This is a vital observation which indicates that the single phase assumption is also capable of providing acceptable results.

The number of investigations about heat transfer enhancement of different nanofluids are also supernumerary, a brief compendium of which is presented by Wang and Mujumdar [12] that includes but not limited to numerical investigations and also review of some classical theories.

1.4 State of the Art on Simulation of Rod Bundles

In order to validate CFD methodology for simulating steady state, single phase flow downstream of structural grids with mixing devices in PWR fuel assemblies, Conner et al. [13] carried out numerical investigations using a commercial CFD package titled "Star-CCM+". In order to provide confidence in their CFD methodology, scaled experiments were performed with a 5×5 rod bundle which is a mimic of a 17×17 full assembly design with rod pitch 12.6 mm, rod diameter 9.5 mm and numerical results were compared against experimental data. For turbulence modeling, the renormalization group (RNG) k-ε model was used and found to produce closest approximation with that of experimental results. It was concluded that proposed CFD model is suitable to predict the behavior of fluid in PWR rod bundle.

Liu & Ferng [14] numerically simulated thermal-hydraulic characteristics including flow, turbulence and heat transfer within the fuel rod bundle with a rod diameter 9.5 mm, heated length 104.1 cm positioned in a square array with a pitch of 1.3 mm. Two different grid designs were considered including the standard grid and split-vane pair one and for turbulence modeling Reynolds Stresses model was used. The simulation conditions were summarized as that inlet temperature was set to 300 K, with an inlet velocity 2.5 m/s (corresponding Re = 28,000) and a constant heat flux of 1.1 MW/m^2. Finally, it was concluded that the grid with split-vane would cause the more turbulent mixing which in turn resulting in the enhancement of fluid heat transfer.

Very recently, Palandi et al. [15] numerically compared the thermo-hydraulic performance of nanofluids and mixing vanes in a triangular assembly using an open-source CFD package Open FOAM for VVER-440 rod bundle which contains 60 fuel rods. The height of the fuel rod bundle is 960 mm with a pitch of 12.2 mm and fuel rod outer diameter 9.1 mm. There are 4 spacer grids with a pitch of 240 mm. The hydraulic diameter of the bundle is 7.782 mm and the simulating environment consists of coolant velocity 3.25 m/s at a temperature 540 K, with a turbulence intensity 3.5% and a constant heat flux of about 1,047,340 W/m^2. Two phase mixture model is used to evaluate the thermo-hydraulic behavior of nanofluid in rod bundle. The results revealed that while by using nanofluid heat transfer coefficient can be increased up to 58%, putting mixing vanes on spacer grids lead to heat transfer enhancement of about 8% only. Hence, it was concluded that from the thermal performance point of

view, use of nanofluid is more effective than putting mixing vanes on spacer grids.

Despite numerous studies including both scaled experiments and numerical modeling on heat transfer enhancement of nanofluids are available in literature, most of them were conducted for a round pipe and also their simulating parameters does not reflect the environment of a nuclear power reactor. Moreover, Wu and Trupp [16] clearly demonstrated that flow conditions inside the fuel rod assembly are quite different from those in typical pipes. There is no appropriate correlation presented yet that can predict heat transfer characteristics of nanofluid in a fuel rod assembly under PWR operating condition. Therefore, in this study a numerical modeling has been performed using a commercial CFD code named "STAR-CCM+ (ver.9.06.011)" with a view to develop a correlation for evaluating Nusselt number with greater accuracy in a square array subchannel for different volume concentrations of water/ alumina (Al_2O_3) nanofluid. In designing the computational domain and fixing simulating variables, a Korean standard nuclear power plant, "APR-1400" has been considered as reference plant. Details of numerical modeling and outcomes including thermo-physical properties of water/ alumina (Al_2O_3) nanofluid are discussed in detail in the subsequent chapters.

Chapter 2. Overview of Nanofluid Heat Transfer

In order to investigate the heat transfer performance of nanofluids and also to implement them in practical applications, it is necessary first to understand the mechanisms involved in heat transfer enhancement process as well as to evaluate different thermo-physical properties of nanofluids such as density, specific heat, viscosity and thermal conductivity. Several mechanisms have been proposed until now to elucidate thermal conductivity enhancement of nanofluids which can be ramified as either static or dynamic models. Details of different heat transfer mechanisms involved and parameters affecting enhancement of thermal conductivity have been described in the following sections of this chapter.

2.1 Parameters Affecting Thermal Conductivity of Nanofluids

It is experimentally proved that thermal conductivity of nanofluids varies with multifarious parameters such as particles volume fraction, particle material, particle size, particle shape, types of base fluid, temperature, pH value of solution, clustering etc. Amounts and types of additives added to prepare the solution also affects the thermal conductivity to a great extent. Since, explaining all of the above parameters is beyond the scope of this study, effects of few most important parameters will be presented here.

2.1.1 Effect of Particle Volume Fraction (φ)

Masuda et al. [17] was the first to experimentally measure the thermal conductivity of three different types of nanofluids containing Al_2O_3 (13 nm), SiO_2 (12 nm), and TiO_2 (27 nm) nanoparticles, whereas water was used as a base fluid. An enhancement as high as 32.4% was observed for the effective thermal conductivity of 4.3 vol.% Al_2O_3/ water nanofluid at 31.85°C and it was concluded that thermal conductivity enhancement increases linearly with particle volume fraction. Later Lee et al. [18] and Wang et al. [19] also conducted similar experiments with different size of Al_2O_3 and CuO nanoparticles and observed similar trends of thermal conductivity enhancement with increment of particle volume fraction.

However, there are also some paradigms of nonlinear behavior. One such study was performed by Murshed et al. [20] who measured the thermal conductivity of TiO_2/ deionized water nanofluid at room temperature by using transient hot-wire method for a volume fraction of nanoparticles varied between 0.5 and 5% and observed a nonlinear relationship was observed between thermal conductivity ratio and particle volume fraction, especially at low volume fractions.

2.1.2 Effect of Base Fluid

The thermal conductivity of nanofluid is also affected by the thermal conductivity of the base fluid. According to the conventional thermal conductivity model proposed by Maxwell [21], thermal conductivity ratio, defined as the thermal conductivity of nanofluid divided by thermal

conductivity of base fluid, increases with the decrease of thermal conductivity of base fluid. Later, Xie et al. [22] performed experiments with alumina nanofluids prepared by using different base fluids e.g. deionized water, glycerol, ethylene glycol, and pump oil. In addition, ethylene glycol-water and glycerol-water mixtures with different volume fractions were also used as base fluids and the variation of the thermal conductivity ratio with thermal conductivity of the base fluid mixture was examined. The results revealed that thermal conductivity ratio decreased with increasing thermal conductivity of the base fluid and experimental results were in fair agreement with the Maxwell model. Chopkar et al. [23] also analyzed the effect of base fluid by comparing water and ethylene glycol and it was found that water-based nanofluids showed a higher thermal conductivity ratio.

2.1.3 Effect of Particle Size

Another pivotal parameter that affects the thermal conductivity of nanofluid is the particle size. Eastman et al. [24] studied Cu nanoparticles (smaller than 10 nm), with ethylene glycol as the base fluid and concluded that the size of the nanoparticles is an important factor that affects the thermal conductivity enhancement, which contradicts the predictions of conventional models such as Hamilton and Crosser model [25], which does not take into account the effect of particle size on thermal conductivity enhancement.

Beck et al. [26] performed a systematic study to check the dependence of thermal conductivity on particle size with Al_2O_3/ water and Al_2O_3/ ethylene glycol nanofluids. Particle size was varied between 8 and 282 nm and HCl was

added to the nanofluids to adjust the pH value to 4. Conductivity measurements were carried out by a transient hot-wire method at room temperature. It was observed that for the same particle volume fraction, thermal conductivity ratio decreases with decreasing particle size. This effect is more pronounced for nanofluids with particles smaller than 50 nm. These results are not in agreement with the above mentioned studies. The results also contradict with the effect of Brownian motion, since the effect of Brownian motion decreases with increasing particle size, which decreases the associated thermal conductivity enhancement.

2.1.4 Effect of Temperature

The thermal conductivity of nanofluid is also subject to change of temperature since it affects the Brownian motion and clustering of nanoparticles [27]. Masuda et al. [17] measured the thermal conductivity of water-based nanofluids containing Al_2O_3, SiO_2, and TiO_2 nanoparticles at different temperatures and observed that thermal conductivity ratio decreased with increasing temperature. Later Das et al. [28] studied the temperature dependence of the thermal conductivity of Al_2O_3 (38.4 nm)/ water and CuO (28.6 nm)/ water nanofluids for different temperatures varying from 21 ^{0}C to 51 ^{0}C and for volume concentrations between 1% and 4% and a linear relationship between thermal conductivity ratio and temperature was observed.

2.2Thermal Conductivity Enhancement Mechanisms of Nanofluid

Several mechanisms have been proposed until now to elucidate the thermal conductivity enhancement of nanofluids. Most of these models can be categorized either as static or dynamic model. While static models presume that nanoparticles are stationary in the base fluid and thus forms a composite material, dynamic models portray that nanoparticles are in constant random motion in the base fluid (termed as Brownian motion) which is the key reason of elevated thermal properties of nanofluid. A short descriptions of different mechanisms involved in heat transfer enhancement of nanofluids are presented below.

2.2.1 Brownian Motion

Brownian motion is defined as the random motion of particles suspended in a fluid as depicted in Fig. 2.1. In case of nanofluids, this random motion transports energy directly by nanoparticles. Bhattacharya et al. [29] used Brownian dynamics simulation to determine the effective thermal conductivity of nanofluids, by considering the Brownian motion of the nanoparticles. It was found that conduction-based Hamilton and Crosser model under predicted the effective thermal conductivity of the nanofluid, since it does not take into account the Brownian motion of the particles within the base fluid.

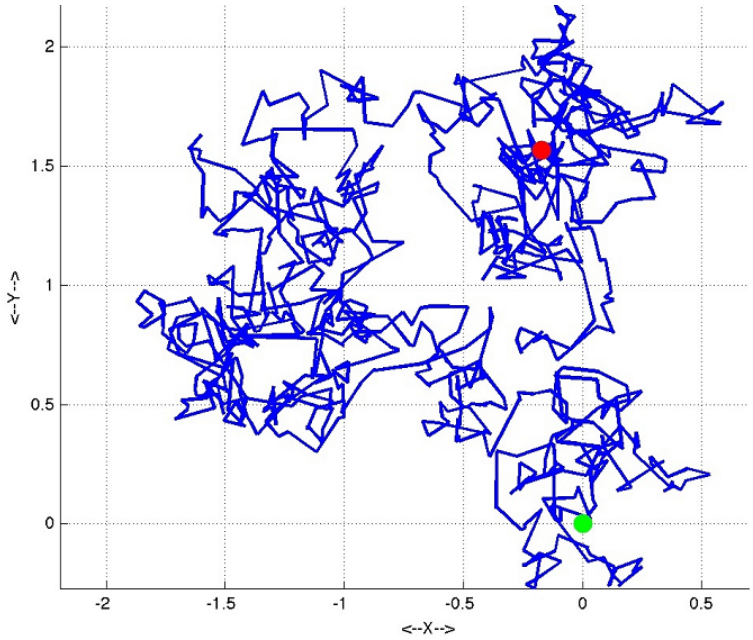

Fig. 2.1: Interpretation of Brownian motion

(Source: https://people.sc.fsu.edu/~jburkardt/m_src/m_src.html)

Prasher et al. [30] presented an analogy between the effect of transitional Brownian motion and convection induced by Brownian motion by considering the existence of an inter-particle potential. The authors concluded that convection in the liquid induced by Brownian motion of nanoparticles was mainly responsible for the anomalous thermal conductivity enhancement of nanofluids. Another study conducted by Li and Peterson [31] also revealed that the mixing effect created by the Brownian motion of the nanoparticles is an important reason for the large thermal conductivity enhancement of nanofluids. Later Jang and Choi [32] developed a model that takes into account convective heat transfer induced by Brownian motion of nanoparticles. The four modes of energy transport in nanofluid introduced by them are as follows:

- Collision between base fluid molecules
- Thermal diffusion in nanoparticles in base fluid
- Collision between nanoparticles due to Brownian motion
- Thermal interaction of dynamic nanoparticles with base fluid molecules.

However, there are also some literatures that described that Brownian motion is not very effective in thermal conductivity enhancement. As for example, Keblinski et al. [33] proposed four possible ways of heat transfer enhancement mechanism by nanofluids one of which was Brownian motion. Nevertheless, they concluded that since a particle may travel across a larger distance over many different paths to reach a final destination that may be very short from the starting point, Brownian motion cannot be the pivotal factor to ameliorate heat transfer, no matter how agitated or energetic they may be. In another study, Evans et al. [34] theoretically showed that the thermal conductivity enhancement due to Brownian motion is a very small fraction of the thermal conductivity of the base fluid. This fact was also verified by molecular dynamics simulations. As a result, it was concluded that Brownian motion of nanoparticles could not be the main cause of anomalous thermal conductivity enhancement with nanofluids.

2.2.2 Clustering of Nanoparticles

Evans et al. [35] proposed due to clustering, fast transport of heat along relatively large distances is possible since heat can be conducted much faster by solid particles when compared to liquid matrix. This phenomenon is

illustrated schematically in Fig. 2.2. In another study conducted by Keblinski et al. [36] also proposes the clustering effect as the main reason of thermal conductivity enhancement. Experimental data for thermal conductivity of nanofluids were analyzed and the potential mechanisms of anomalous enhancement were examined and it was concluded that enhancement mechanisms such as micro-convection created by Brownian motion of nanoparticles, nanolayer formation around particles, and near field radiation were not to be the major cause of the enhancement. Feng et al. [37] also concluded that due to effect of clustering thermal conductivity of nanofluid is augmented which is more pronounced in nanofluids with smaller nanoparticles since distances between nanoparticles are smaller in those nanofluids, which increases the importance of van der Waals forces attracting particles to each other.

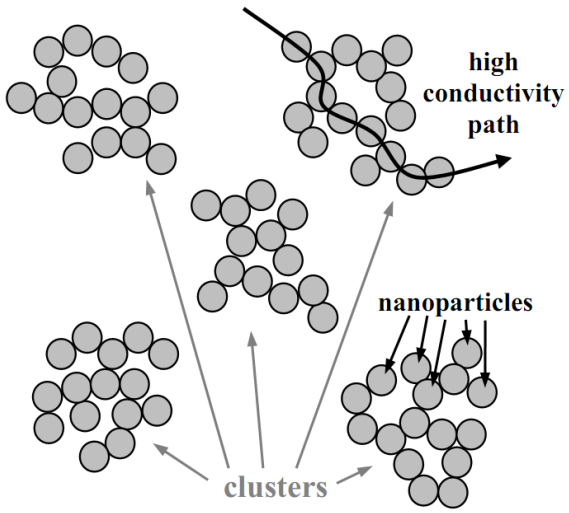

Fig. 2.2: Schematic representation of the clustering phenomenon [38]

2.2.3 Liquid Layering around Nanoparticles

A recent research conducted by Yu et al. [39] showed that nano-layered structures around solid surfaces are formed by liquid molecules and it is anticipated that those layers have larger effective thermal conductivity than the liquid matrix [40]. This phenomenon is illustrated schematically in Fig. 2.3.

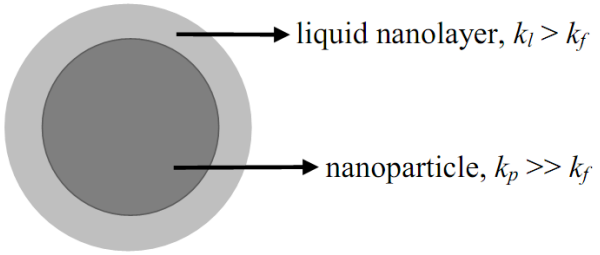

Fig. 2.3: Illustration of liquid layering around nanoparticles. k_l, k_f, and k_p are thermal conductivity of nanolayers, base fluid and nanoparticles respectively[41]

2.2.4 Ballistic Phonon Transport in Nanoparticles

Keblinski et al. [42] estimated the phonon mean-free path of Al_2O_3 nanoparticles at room temperature and indicated that ballistic heat transport can create a significant effect on thermal conductivity of nanofluids if it enables efficient heat transport between nanoparticles. This is only possible if the nanoparticles are very close to each other (a few nanometers separated) and they noted that this is the case for nanofluids with very small nanoparticles. Furthermore, the authors stressed on the fact that the particles may become closer to each other due to the Brownian motion.

2.2.5 Near Field Radiation

The effect of near field radiation on the heat transport between two nanoparticles was investigated by Domingues et al. [43]. The results delineated that when the distance between the nanoparticles is smaller than the diameter of the particles, the heat conductance is two to three orders of magnitudes greater than the heat conductance between two particles that are in contact. Besides, Brownian motion of nanoparticles can also improve that mechanism since the distance between nanoparticles changes rapidly due to the random motion.

2.3 Effect of Particle Deposition of Heater Surface

The effect of nanoparticles deposition on heater surface was studied by many researchers who have conducted experiments on nanofluid boiling, both pool and convective. While this is considered as the pivotal reason behind the critical heat flux (CHF) enhancement, it is observed that convective heat transfer coefficient, h ($W/m^2.K$) of nanofluid is not affected by nanoparticle deposition on heater rod surface.

Ahn et al. [44] performed experiments with aqueous nanofluids with a 0.01% concentration of alumina nanoparticles under forced convective flow conditions with different velocities spanning from 0 m/s (effectively pool boiling) to 4 m/s; a CHF enhancement of 50% was observed at 0 m/s compared to that of pure water. Later, a scanning electron microscope (SEM) was used to examine the heater surfaces and it was observed that nanoparticle deposition on heater surface caused the contact angle to decrease from 65^0 to about 12^0,

illustrating an evident enhancement in the surface wettability which primarily contributed to the CHF enhancement. The surface wettability affects the CHF; CHF occurs when dry patches (hot spots) develop on the heater surface at high heat fluxes; these dry spots can be rewetted or can irreversibly overheat, causing CHF. Therefore, an increase in surface wettability promotes dry-spot rewetting and thus delaying CHF.

In another experiment, Kim et al. [45] measured both the CHF and the heat transfer coefficient in flow boiling condition using dilute alumina, zinc oxide and diamond water-based nanofluids. CHF enhancement was found to increase with both mass flux and nanoparticle concentration for all nanoparticle materials; and they also reached at the same conclusion as Ahn et al. [44]. Moreover, using confocal microscopy, they measured the number of micro-cavities on the surface and the contact angle of the fluid on surface, and thus obtained an estimation of the nucleation site density at the heater surface but no definitive correlation could be found between the nucleation site density and convective heat transfer data. Hence, it was concluded that the nanoparticles must affect the convective heat transfer coefficient via some other mechanisms, unidentified at this time.

2.4 Chemical and Physical Stability of Nanofluid

One central property that must be taken into consideration to utilize nanofluid as a coolant in PWRs is its chemical and physical stability under typical PWR water chemistry. Most researches are initially focused on using nanofluid coolant only in PWRs, since BWRs does not seem very promising

due to carry over of nanoparticles to the secondary side of the plant and thus creating corrosion, erosion and fouling in turbine and condensers. From the literatures cited in earlier sections of this study, it is clear that agglomeration can increase the size of particles and thus the probability for gravity and inertial deposition can be increased to a great extent. Despite dilute solutions of nanoparticles tends to show more stability, however, in case of long term use, even in dilute solutions thermal agitation and flow mixing are not sufficient to prevent agglomeration [1].

However, it is experimentally proved that in nanofluids with oxide nanoparticles, agglomeration can be largely abated by adjusting the pH of solution to create like electric charges on the nanoparticles surface so that the nanoparticles repels each other on contact. Nevertheless, in PWR water chemistry, pH is an instrumental parameter in mitigating corrosion and typical value to keep corrosion within a certain range is 6.9 to 7.4 at room temperature. Therefore, it is of utmost importance to discover a suitable nanofluid that will be stable within the same allowable pH range, as changing the PWR water chemistry to accommodate the nanofluid coolant will not be feasible. Moreover, the surfactants may also undergo severe radiolysis when exposed to core radiation, and thus not fulfill their intended purpose. Hence, it can be concluded that much more investigations are required in this arena, including study of radiation effects on nanofluid stability, as well as the impact of nanoparticle deposition on corrosion behavior of fuel rod cladding materials.

Chapter 3. Overview of CFD and Star-CCM+

3.1 Definition of CFD

Computational fluid dynamics, abbreviated as CFD is the method of analyzing systems that involves fluid flow, heat transfer and related phenomena such as chemical reactions by means of a powerful computer aided simulation [46]. In CFD, a discretization method is used to obtain an approximate numerical solution, which approximates the differential solutions by a system of algebraic equations, which can then be solved by a computer. The accuracy of numerical solutions is directly dependent on the quality of discretization used. In general, the process of CFD can be best described by means of following diagram:

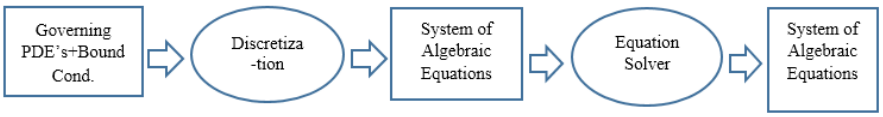

Fig. 3.1: Process involved in CFD [47]

3.2 Governing Equations of CFD

In CFD, the cornerstone is nothing but the governing equations of fluid dynamics representing mathematical statements of the conservation laws of physics:

- The mass of fluid is conserved.
- The rate of change of momentum equals the sum of forces on a fluid particle (Newton's second law).

- The rate of change of energy is equal to the sum of the rate of heat addition to and the rate of work done on a fluid particle (First law of thermodynamics).

In our present study, the flow inside the subchannel has been considered as single phase and incompressible with constant physical properties and also both the compression work and viscous dissipation have been assumed as negligible. Under such conditions, the general conservation equations of mass, momentum and energy can be written in the form of Eq. (3.1) through (3.3) respectively using vector notations [9]:

$$\mathrm{div}\left(\rho v\right)=0 \tag{3.1}$$

$$\mathrm{div}\left(\rho vv\right)= -\mathrm{grad}P+\mu\Delta^2 v \tag{3.2}$$

$$\mathrm{div}\left(\rho vC_P T\right)= \mathrm{div}\ \left(k\ \mathrm{grad}T\right) \tag{3.3}$$

In above equations, *v*, *P* and *T* are fluid velocity vector, pressure and temperature respectively.

3.3 Elements of a CFD Code

The three instrumental elements of any CFD codes that are commercially available today are following:

- Pre-processor
- Solver and
- Post-processor

3.3.1 Pre-processor:

It provides a user friendly graphics interface to input a flow problem in a CFD program and subsequent transformation of that input into a suitable form to be used in solver. The key tasks performed in this stage are following:

- Create/ import a geometry of the region of interest, i.e. computational domain
- Discretization of geometry into computational meshes, i.e. grid generation
- Defining physics of the problem that needs to be modelled
- Defining fluid properties
- Defining appropriate boundary conditions

3.3.2 Solver:

The three distinct pillar of numerical techniques are: Finite Difference Method (FDM), Finite Volume Method (FVM) and Finite Element Method (FEM), among which FVM is the central to the most of the well-known CFD codes which are commercially available: ANSYS/CFX, FLUENT, Star-CCM+, PHOENICS etc. In FVM, solution algorithm consists of the following steps:

- Integration of governing equations of fluid dynamics over all (finite) control volumes of the computational domain.
- Discretization- conversion of resulting integral equations into a system of algebraic equations.
- Solution of algebraic equations by an iterative procedure.

In short, the process of obtaining a practical solution about problems related to fluid motion in CFD can be delineated as follows:

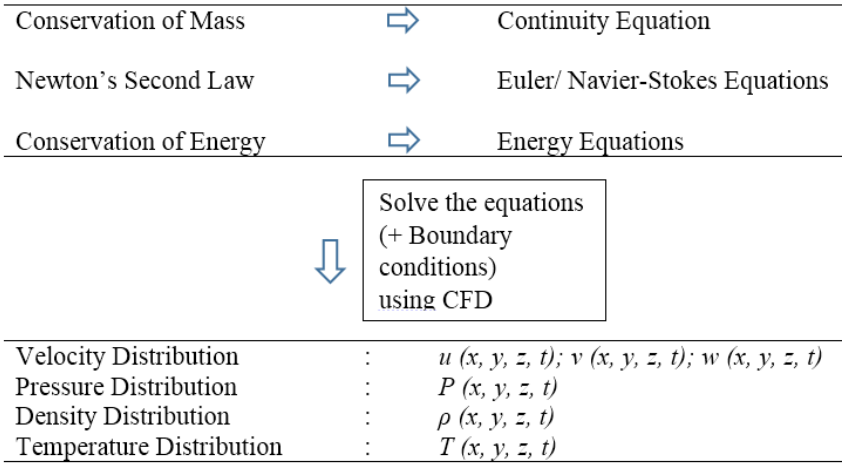

Fig. 3.2: Process of obtaining solution in CFD [47]

3.3.3 Post-processor:

Last but not least, the leading CFD packages provides outstanding graphics and data visualization tools which includes but not limited to:

- Domain geometry and mesh display
- Vector, line and shaded contour plots
- 2D and 3D surface plots
- Particle tracking
- View manipulations (translation, rotation, scaling etc.)
- Color Postscript output

More recently, animation for dynamic result display has also been included. The graphics output capabilities of CFD code thus have brought a revolutionary change in communicating ideas to the non-experts.

3.4 Properties of Numerical Solutions

In order to produce a meaningful result, the numerical solution should have some properties among which the most important ones are summarized below:

3.4.1 Consistency:

A numerical method is said to be consistent if the truncation error (which is the difference between discretized equation and the exact solution) tends to become zero when the grid spacing $\Delta t \rightarrow 0$ and/ or $\Delta x_i \rightarrow 0$. However, there is no guarantee that the solution of the discretized equation system will become the exact solution of differential equations even if the method is consistent, for which the solution needs to be stable too.

3.4.2 Stability:

A numerical solution is termed as stable if the errors results from series of numerical solution process are not amplified in the ongoing further steps. For iterative solutions, a stable method is one which does not diverge with time. The stability of a numerical solution can be characterized by the Courant-Friedrichs-Levi condition (CFL number) defined as follows:

$$CFL = u\frac{\Delta t}{\Delta x} \tag{3.4}$$

Where, u is the characterized velocity, Δt is the time step and Δx is the grid size. The higher the value of CFL number, the more likely is that the method is instable. While for an explicit scheme, CFL value less than unity is

desirable, implicit schemes are more stable and can accept CFL value greater than 1.

3.4.3 Convergence:

A numerical methods is said to achieve convergence if the solution of discretized equations tends to the exact solutions of the governing differential equations as the grid spacing tends to zero. Obviously a consistent scheme is of no use unless the method converges. For non-linear problems which are strongly dependent on boundary conditions, convergence is checked by performing numerical experiments on a series of successive refined grids. If the method is convergent, it will lead to a grid independent solution.

3.4.4 Conservation:

Since the basic equations that are solved in any numerical scheme are basically conservation equations, the discretized equations should also pay tribute to these laws which means at steady state and in absence of sources, the amount of a conserved quantity leaving a closed volume should be equal to the amount entering that volume. If this property is conserved, it can be anticipated that truncation error consists of only inaccurate distribution of fluid properties over the computational domain.

3.4.5 Boundedness:

It refers that physically non-negative properties like density, kinetic energy of turbulence etc. should be always positive and other quantities like

concentration should be between 0% and 100%. Despite boundedness is difficult to guarantee, it usually happens only if the grid size is too coarse.

3.4.6 Realizability:

It means that while modeling a complex phenomenon, such as turbulence, combustion or multiphase flow, one should be able to define a numerical scheme that will properly reflect the real physics of the problem and thus will obtain realistic solution.

3.5 Introduction to Star-CCM+

Star-CCM+ is a powerful CFD code developed by CD-Adapco since 2004 to introduce an easy-to-use engineering tool that combines automatic meshing with extensive modeling and post-processing capabilities not only reserved for CFD experts. The last part of the name –CCM- is derived from Computational Continuum Mechanics and hence, the outstanding features that has made this CFD package unique from others are following:

- Multi-Physics, continuum-based modeling
- Separation of Physics and Mesh
- Generalized interfaces
- Face-based solver: any cell type is supported
- Full interactive control over simulation process
- Full process integration: CAD to CAE in one package
- Capable of handling very large models (100M+ cells)
- Last but not least, based on latest numerics and software technologies

Star-CCM+ works based on Finite Volume Method (FVM), which means it converts volume integrals into surface integrals by implementing divergence theorem, and then by using proper initial and boundary conditions and a number of discretized approximations, an algebraic system of equation is solved on a computer. The basic workflow of Star-CCM+ is shown in the following figure:

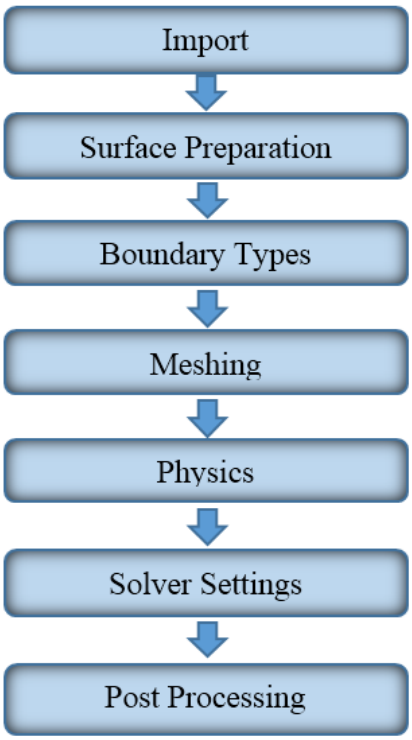

Fig. 3.3: Overview of workflow in Star-CCM+ [48]

Chapter 4. Methodology of Numerical Modeling

4.1 Determination of Physical Properties of Nanofluid

Determination of physical properties of nanofluid like density, specific heat, viscosity and thermal conductivity is key to any nanofluid research. If the nanoparticles are assumed to be well dispersed in the base fluid; the particle concentration can be considered as constant throughout the domain and effective physical properties of mixture can be evaluated using some classical formulas well known for two phase fluids [9]. In this study, formulas used to determine different properties of nanofluid are presented below:

- **Density:**

$$\rho_{nf} = (1-\varphi)\rho_{bf} + \varphi\rho_P \tag{4.1}$$

- **Specific Heat:**

$$(C_P)_{nf} = (1-\varphi)(C_P)_{bf} + \varphi(C_P)_P \tag{4.2}$$

- **Dynamic Viscosity:**

$$\mu_{nf} = \left(1 + 7.3\varphi + 123\varphi^2\right)\mu_{bf} \tag{4.3}$$

- **Thermal Conductivity:**

$$k_{nf} = \left(1 + 2.72\varphi + 4.97\varphi^2\right)k_{bf} \tag{4.4}$$

Eq. (4.1) and (4.2) are general relationships have been used in many literatures [3, 9, 11] to recon the density and specific heat for a classical two phase mixture. Regarding dynamic viscosity, Maïga et al. [49] showed that,

despite some correlations exists to claculate dynamics viscosity of nanofluid as proposed by Einstein and later improved by Brinkman [50] and another one proposed by Batchelor [51], these formulas drastically underestimate the viscosity of nanofluids. Therefore, they performed a least-square curve fitting based on some scarce experimental data available in [17-19] which lead to Eq. (4.3). In case of thermal conductivity, the same situation prevails like dynamic viscosity, thereby introducing Eq. (4.4) as presented in [9, 52]. Despite the experimental condition i.e. pressure and temperature of above investigations are quite different from the operating condition of a PWR, since there exists no such correlation for thermophysical properties of nanofluid which is derived in the operation environment of a PWR, it is assumed that mentioned correlations can also be utilized for nuclear applications. Different properties of base fluid (pure water) and alumina nanoparticles that have been used in this study are tabulated in Table 4.1.

Table 4.1: Physical properties of base fluid and alumina nanoparticles

Properties	Base Fluid (Pure Water)	Alumina Nanoparticles
Density (kg/m^2)	734.928	3970
Thermal Conductivity ($W/m^2.K$)	0.5701	40
Specific Heat (J/kg. K)	5361.69	880
Dynamics Viscosity (Pa. s)	9.01373E-05	-

4.2 Methodology of Numerical Modeling

In this study, a commercial CFD software "Star-CCM+ (ver. 9.06.011)" designed by CD-Adapco has been used for modeling flow through a square array subchannel using pure water and different volume concentrations of water/alumina (Al_2O_3) nanofluid. Details of the numerical procedure including validation of model has been described in the following sections:

4.2.1 Computational Domain

The computational domain and boundaries considered for this study is shown in Fig. 4.1, which represents quarter of a 3-D square array subchannel created in Star-CCM+. The diameter of the fuel rod is taken as 9.5 mm and two different rod pitch featuring pitch to diameter (*P/D*) ratio of 1.25 and 1.35 are selected for simulation. The length of the subchannel has been taken as 600 mm based on Eq. (4.5) and (4.6) which is long enough to establish a fully developed turbulent flow at outlet under single phase forced convection condition up to $Re = 6\times10^5$.

$$l_e = EI \times D_h \tag{4.5}$$

$$EI = 4.4 \times \mathrm{Re}^{\left(\frac{1}{6}\right)} \tag{4.6}$$

where, l_e is entrance length for fully developed flow, EI is entrance length number and D_h is the channel hydraulic diameter.

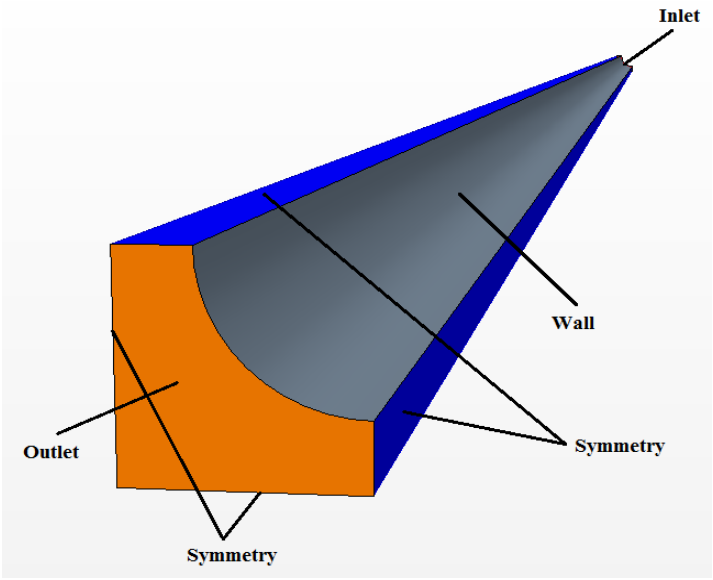

Fig. 4.1: Computational domain created in Star-CCM+

4.2.2 Boundary Conditions

The coolant enters into the subchannel with a uniform inlet velocity, v_0 (m/s) and at inlet temperature 569 K. Different values of v_0 for different coolants that have been used in the simulation are tabulated in Table 4.2. Different properties of base fluid (pure water) have been calculated at temperature 569 K and at pressure 155.1375 Bar. At outlet, a static pressure equal to 155.1375 Bar has been imposed. On the tube wall, the usual non-slip conditions with standard wall function are considered with a constant heat flux of 600,000 W/m^2. The above parameters and geometric configurations of computational domain are based on the design features of a Korean standard nuclear power plant called “APR 1400”.

Table 4.2: Different inlet velocities, v_0 (m/s) used in simulation.

***P/D* = 1.25**

Inlet *Re*	Pure Water (φ=0%)	Alumina (Al_2O_3) Nanofluid		
		φ=0.5%	φ=1.5%	φ=3.0%
6×10^5	7.829	7.963	8.351	9.196
5.098×10^5	6.651	6.766	7.095	7.813
4×10^5	5.219	5.309	5.568	6.130
3×10^5	3.914	3.982	4.176	4.598

***P/D* = 1.35**

Inlet *Re*	Pure Water (φ=0%)	Alumina (Al_2O_3) Nanofluid		
		φ=0.5%	φ=1.5%	φ=3.0%
6×10^5	5.826	5.926	6.215	6.843
5.098×10^5	4.950	5.035	5.280	5.814
4×10^5	3.884	3.951	4.143	4.562
3×10^5	2.913	2.963	3.108	3.422

4.2.3 Physics Set-up

Different physics models needs to be implemented based on what is to be modeled. In this study, simulations are carried out by setting the flow as incompressible, steady and turbulent. Constant density model is chosen for material. For turbulence modeling, realizable k-ε model with high y^+ wall treatment is selected. Implicit coupled solver with second-order upwind discretization scheme in conjunction with coupled energy model is implemented which solves the conservation equations for mass and momentum simultaneously using a pseudo time marching approach. This model is desired

to use for solving complex flows that includes dominant source terms e.g. rotation and heat transfer.

Another optional model, cell quality remediation is also selected to get solutions on a poor quality mesh. This model identifies poor-quality cells, using a set of predefined criteria, such as skewness angle exceeding a certain threshold. Once these cells and their neighbors have been marked, the computed gradients in these cells are modified in such a way as to improve the robustness of the solution.

4.2.4 Selection of Turbulence Model

By studying different literatures on numerical simulation of flow through a rod bundle for nuclear applications, it can be concluded that no specific turbulence model can be regarded as superior to others for this sort of flow phenomena. Yadigaroglu et al. [53] carried out an exhaustive review of rod bundle numerical simulations and opined that the gradient transport models, like the standard k-ε model, are not capable of predicting turbulent flow in the narrow gap regions. Hàzi [54] had demonstrated that the Reynolds Stress Model (RSM) could be accurately applied in simulating the rod bundle geometry. Lee and Choi [55] also used the RSM turbulence model to compare the performance of grid designs between the small scale vortex flow (SSVF) mixing vane and the large scale vortex flow (LSVF) mixing vane. Liu and Ferng [14] have also adopted RSM turbulence model to numerically investigate the effects of different types of grid (standard grid and split-vane pair one) on the turbulence mixing and heat transfer. Palandi et al. [15] have successfully implemented SST

k-ω model in comparing thermo-hydraulic performance of nanofluids and mixing vanes in VVER-440 triangular array fuel rod bundle. However, application of RSM turbulence model will require 50-60% more CPU time per iteration compared to standard *k-ε* and *k-ω* model and 15-20% more memory usage.

Recently Conner et al. [13] have implemented renormalization group (RNG) *k-ε* model (Yakhot et al., [56]) in simulation a 5×5 rod bundle with mixing-vane grid using Star-CCM+. The applicability of this model to simulate fuel rod bundles has been tested and validated by Westinghouse in their extensive research (Smith et al., [57]).

Considering the established practice and computational time required as discussed above, it can be concluded that RNG *k-ε* model will be suffice in modeling turbulence for flow through a rod bundle. However, in this study, realizable *k-ε* model (Shih et al., [58]) has been adopted for turbulence modeling inside a square array subchannel since it has been statistically proved that this model provides the best performance among all the *k-ε* model versions for separated flows and flows with complex secondary flow features [59].

The term “realizable” means that the model satisfies certain mathematical constraints on the Reynolds stresses, consistent with the physics of turbulent flows. Neither the standard *k-ε* nor the RNG *k-ε* model is realizable.

The modeled transport equation for k and ε in the realizable k-ε model are:

$$\frac{\partial}{\partial t}(\rho k)+\frac{\partial}{\partial x_i}(\rho k u_j)=\frac{\partial}{\partial x_i}\left[\left(\mu+\frac{\mu_t}{\sigma_k}\right)\frac{\partial k}{\partial x_j}\right]+G_k+G_b-\rho\varepsilon-Y_M+S_k \quad (4.7)$$

and

$$\frac{\partial}{\partial t}(\rho\varepsilon)+\frac{\partial}{\partial x_j}(\rho\varepsilon u_j)=\frac{\partial}{\partial x_i}\left[\left(\mu+\frac{\mu_t}{\sigma_\varepsilon}\right)\frac{\partial \varepsilon}{\partial x_j}\right]+\rho C_1 S_\varepsilon-\rho C_2\frac{\varepsilon^2}{k+\sqrt{\nu\varepsilon}}+C_{1\varepsilon}\frac{\varepsilon}{k}C_{3\varepsilon}G_b+S_\varepsilon \quad (4.8)$$

$$C_1=\max\left[0.43,\frac{\eta}{\eta+5}\right] \quad (4.9)$$

$$\eta=S\frac{k}{\varepsilon} \quad (4.10)$$

In above equations, G_k represents the generation of turbulence kinetic energy due to mean velocity gradients, G_b is the generation of turbulence kinetic energy due to buoyancy, Y_M is the contribution of fluctuating dilatation in compressible turbulence to the overall dissipation rate, C_2 and $C_{1\varepsilon}$ are constants, σ_k and σ_ε are the turbulent Prandtl numbers for k and ε respectively, S_k and S_ε are user-defined source terms.

4.2.5 Convergence of Numerical Solution

Another central criteria that must be satisfied in order to obtain proper numerical solution is convergence. The solver needs to be given adequate iterations so that the problem is converged and a solution can be treated as converged if the following criteria are satisfied [59]:

- The solution no longer changes with subsequent iterations

- Overall mass, momentum, energy and scalar balance are achieved
- All equations (momentum, energy etc.) are obeyed in all cells to a specified tolerance

In the present study, residuals for continuity, X & Y- momentum, Z-momentum and turbulence kinetic energy are decreased respectively to an order of 10^{-2}, 10^{-5}, 10^{-2} and 10^{-4} after 30,000 iterations and also a monitor is created to check how values for mass flow averaged temperature at outlet is converging and it is observed that after 30,000 iterations these values does not change significantly with further iterations. A typical plot of mass flow averaged temperature at outlet for pure water at inlet $Re = 6\times10^5$ is shown in Fig. 4.2:

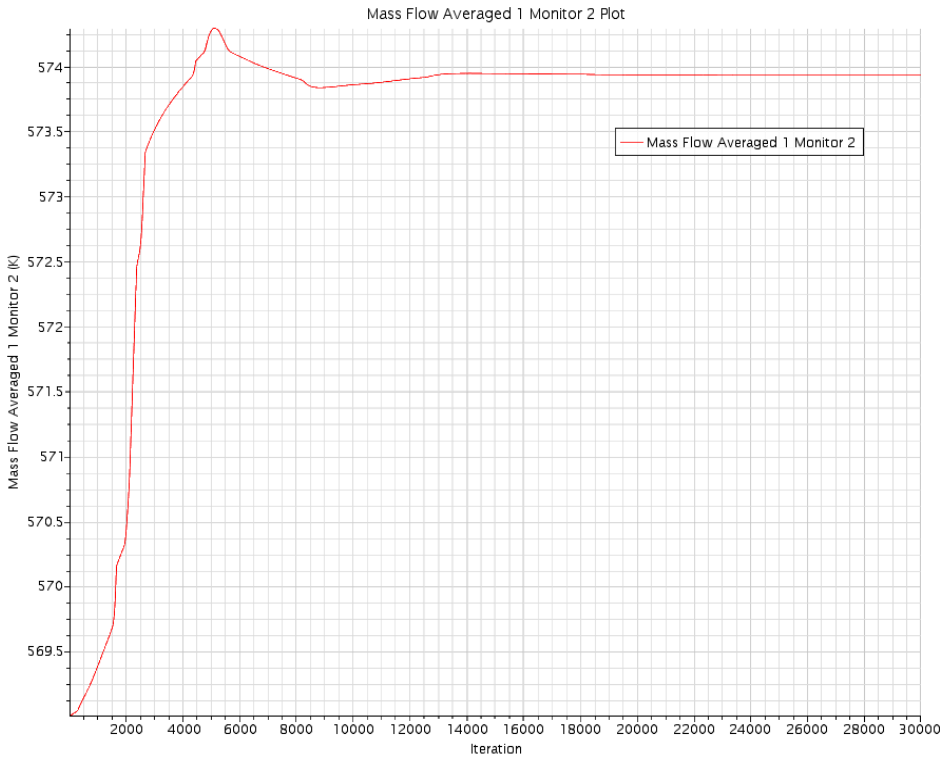

Fig. 4.2: Convergence of mass flow averaged temperature at outlet (P/D = 1.35) for pure water at corresponding inlet $Re = 6\times10^5$

4.2.6 Wall y^+ Values

The accurate calculations of y^+ value in the near-wall region, which is a measure of non-dimensional distance from the wall to the first mesh node (based on local cell fluid velocity), are of paramount importance to the success of any simulation. In order to use a wall function approach properly for a particular turbulence model with confidence, the y^+ values should be within a certain range.

If the y^+ values are too large it indicates that the first node falls outside the boundary layer region and in turn the wall functions used by turbulence model may incorrectly calculate the flow properties at this first calculation point and thus propagating errors into pressure drop and velocity results.

On the contrary, if the y^+ value is too low then the first calculation point is placed in the viscous sub-layer (logarithmic) flow region and the wall functions will also be outside their validity (below about $y^+ < 11$).

In the present study, standard wall function is used in conjunction with realizable k-ε model and high-y^+ wall treatment in which the near-wall cell centroid are anticipated to be placed in the log-law region with a value $30 \leq y^+ \leq 100$. Results of performed simulations demonstrates that the wall y^+ values for different cases are within this specified range. A pictorial representation of wall y^+ in case of pure water with $Re=6\times10^5$ (P/D =1.35) is shown in Fig. 4.3.

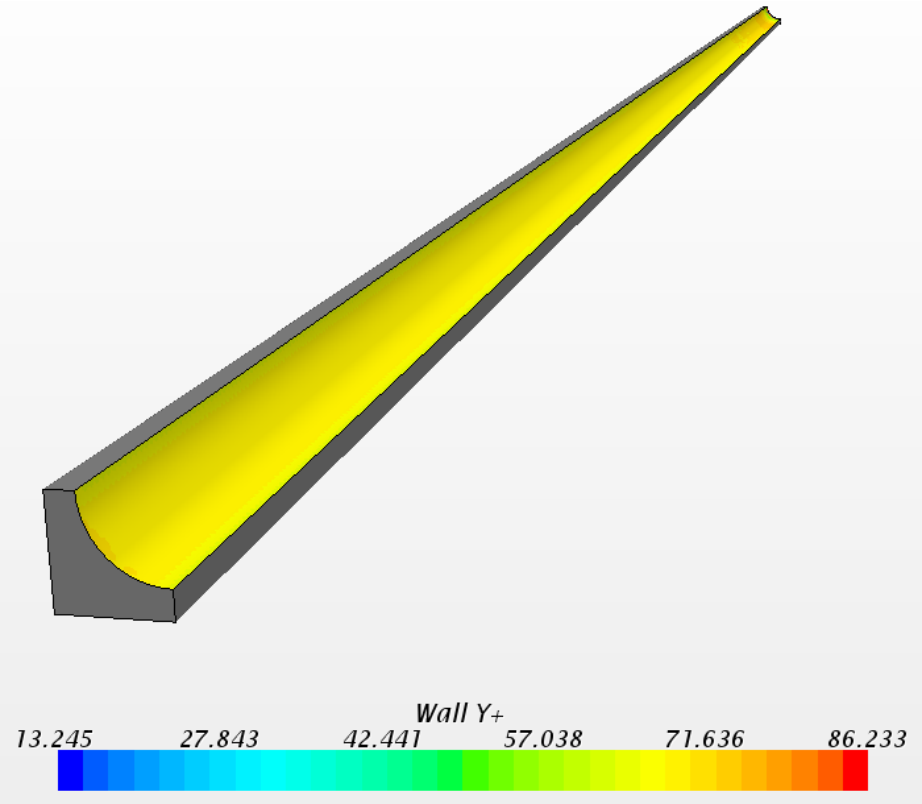

Fig. 4.3: Distribution of wall y+ values in case of pure water with

Re=6×10^5 (P/D =1.35)

Chapter 5. Numerical Results and Discussion

5.1 Mesh Convergence Test

Since the accuracy of finite volume method is directly related to the quality of discretization used, it is instrumental to select an optimized mesh size that will take into account both resolution of mesh structure and as well as computational time and cost.

In the present study, different mesh settings are selected as presented in Table 5.1 and values of numerically obtained *Nu* are compared against an existing correlation for square array subchannel and for pure water as presented by Eq. (5.1) through Eq. (5.3) to check mesh convergence for computational domain with *P/D* =1.35. Results are plotted in Fig. 5.1 which clearly states that a mesh setting with base size 0.7 mm, no. of prism layer 2, prism layer thickness 0.3mm and prism layer stretching 3.7 will be sufficient to produce *Nu* within reasonable deviation compared to theoretical prediction made by correlation.

$$Nu = \psi \left(Nu_{\infty} \right)_{c.t.} \tag{5.1}$$

where,
$$\left(Nu_{\infty} \right)_{c.t.} = 0.023 \,\mathrm{Re}^{0.8} \,\mathrm{Pr}^{0.4} \tag{5.2}$$

for square array with $1.05 \leq P/D \leq 1.9$ and for pure water, Presser [60] suggested:

$$\psi = 0.9217 + 0.1478 \,{}^{P}\!/_{D} - 0.1130 e^{-7\left({}^{P}\!/_{D} - 1\right)} \tag{5.3}$$

Table 5.1: Different mesh settings used to check mesh convergence.

Base Size (mm)	Prism Layers			*Nu* (Star-CCM+)	*Nu* (Presser)	Deviation (%)
	No.	Stretching	Thickness (mm)			
0.5	5	1.5	0.7	742.940	1003.35	-35.051
0.6	4	1.5	0.5	862.627		-16.313
0.7	3	3.8	0.4	933.92		-7.434
0.6	2	3.7	0.3	972.102		-3.214
0.7	2	3.7	0.3	1010.57		0.714

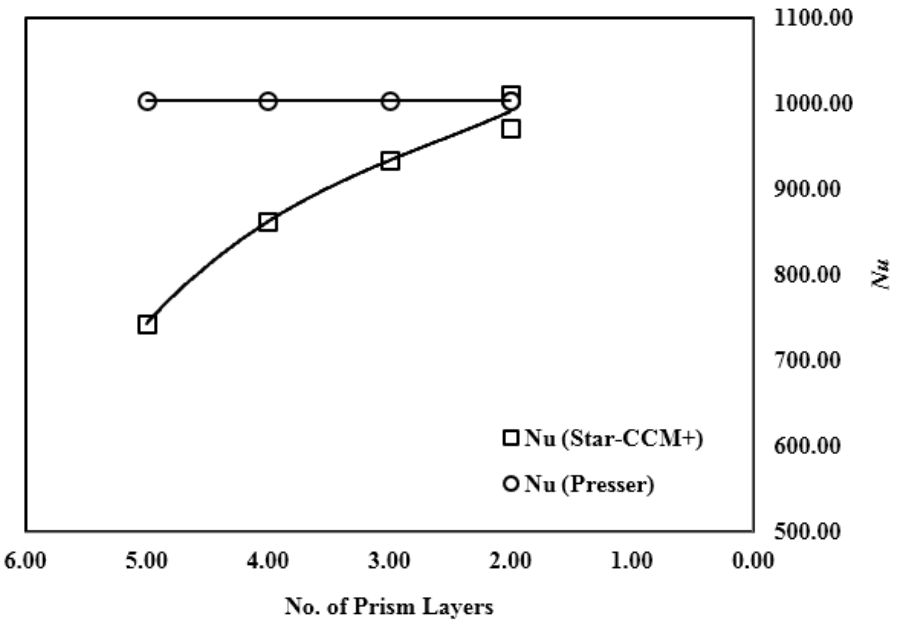

Fig. 5.1: Mesh convergence test with different mesh settings

5.2 Validation of Numerical Model

Since the ultimate test of any numerical simulation is the validation of results against well-known experimental data, the model under consideration in the present study has been validated against correlation of Presser for square array and pure water as presented by Eq. (5.1) through Eq. (5.3). Results are tabulated in Table 5.2 and plotted in Fig. 5.2 and Fig. 5.3 which demonstrates that there is an excellent match between numerical data and theoretical prediction for the specified range of inlet *Re*.

Table 5.2: Validation of numerical model against Presser's correlation.

***P/D* = 1.25**

Inlet *Re*	*Nu*		Deviation (%)
	Star-CCM+	Presser	
6×10^5	988.7949	981.0835	0.7798
5.098×10^5	861.9004	861.1521	0.0868
4×10^5	702.8976	709.3049	-0.9115
3×10^5	551.8459	563.4845	-2.1090

***P/D* = 1.35**

Inlet *Re*	*Nu*		Deviation (%)
	Star-CCM+	Presser	
6×10^5	1010.5676	1003.3492	0.7142
5.098×10^5	880.5523	880.6960	-0.0163
4×10^5	717.4199	725.4026	-1.1126
3×10^5	561.0203	576.2728	-2.7186

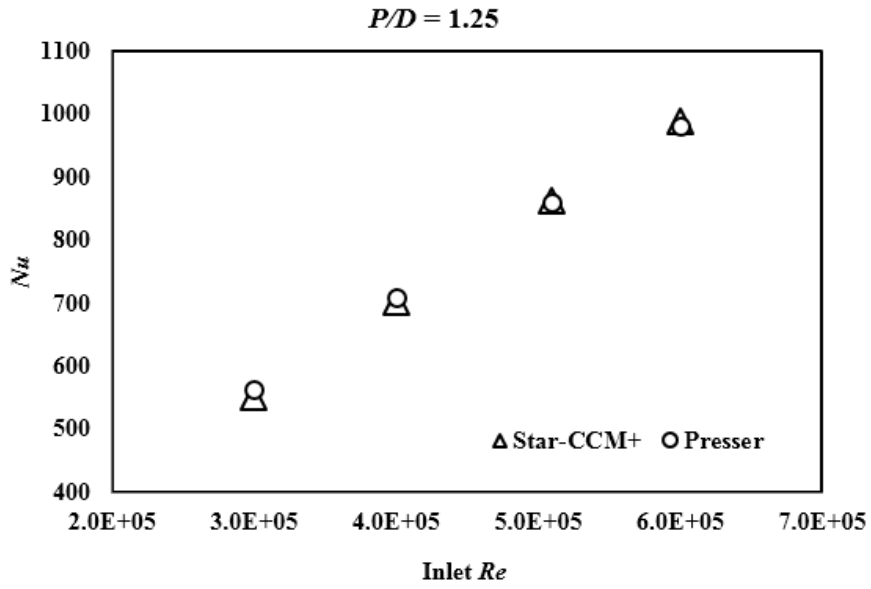

Fig. 5.2: Validation of numerical model against correlation for *P/D* =1.25

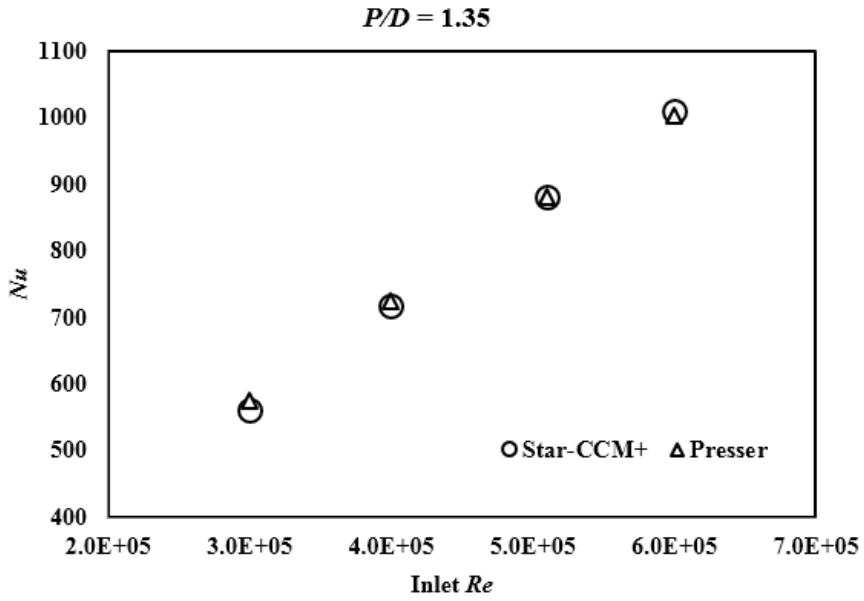

Fig. 5.3: Validation of numerical model against correlation for *P/D* =1.35

5.3 Validation of Turbulence Model for Nanofluid

Most nanofluids intended to use in practical applications are composed of oxide particles smaller than 40 nm. Therefore, Xuan and Roetzel [61] suggested that the particles may be fluidized easily and the mixture would likely to behave as a single fluid rather than heterogeneous mixture. Thus by assuming that nanofluid would behave as a single-phase homogeneous fluid, all equations of conservations (mass, momentum and energy) for single-phase fluids can directly be applied to nanofluids. However, in the present study, realizable k-ε model is adopted due to its simplicity with higher effectiveness and a successful comparison of numerical *Nu* obtained by this model has been carried out against both empirical correlation and experimental data of Pak & Cho [3] for turbulent flow inside a round pipe of inside diameter 10.66 mm using alumina nanofluid (φ=2.78%) as coolant for inlet *Re* spanning from 5.03×10^4 to 1.48×10^4. The results are documented in Table 5.3 and plotted in Fig. 5.4 which clearly delineates that this model can perform quite satisfactorily with nanofluids.

Table 5.3: Validation of turbulence model against Pak & Cho's correlation

Inlet *Re*	*Nu*			Deviation (%)	
	Star-CCM+	Pak & Cho		Correlation	Experiment
		Correlation	Experiment		
5.029×10^4	387.57	398.22	393.59	-2.64	-1.53
3.562×10^4	286.37	302.16	286.17	-5.22	0.067
2.412×10^4	204.17	221.27	223.90	-7.72	-8.81
1.477×10^4	133.90	149.44	141.90	-10.39	-5.63

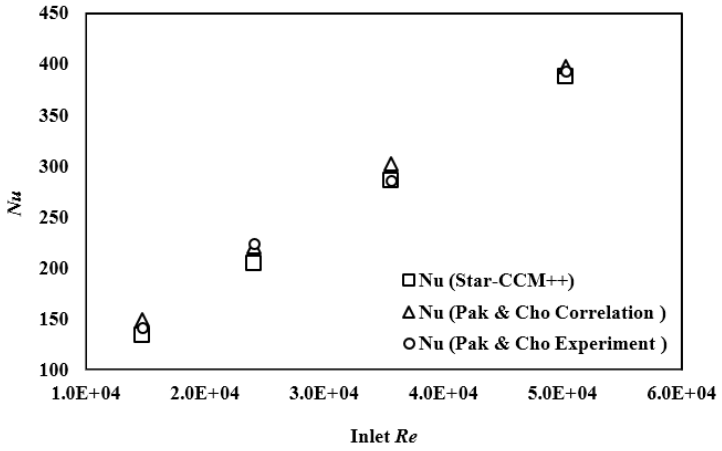

Fig. 5.4: Validation of turbulence model against Pak & Cho's correlation

5.4 Results and Discussion

5.4.1 Temperature

Temperature profile along the centerline of subchannel (*P/D* =1.25) for different coolants at inlet *Re* = 6×10^5 are illustrated in Fig. 5.5 from which it is clear that there is a steady increase in the coolant temperature due to absorption of heat while flowing through the subchannel and bulk temperature of nanofluid is decreased with the increasing particle volume concentration.

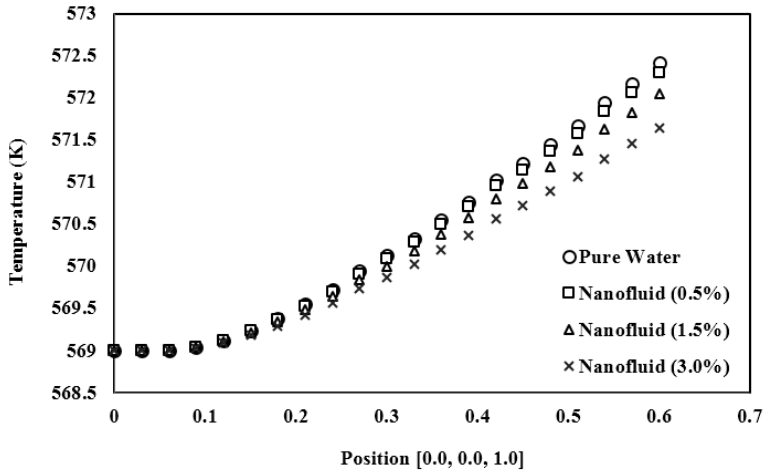

Fig. 5.5: Temperature along centerline of subchannel at *Re* = 6×10^5

5.4.2 Velocity

Development of axial velocity along the centerline of subchannel (*P/D* =1.25) for different coolants at inlet *Re* = 6×10^5 is presented in Fig. 5.6 which clearly states that fully developed velocity profile occurs approximately after z=0.3 m and if the current models are implemented to evaluate physical properties of nanofluid, development of velocity profile is not affected by the inclusion of nanoparticles. From Fig. 5.6, it can also be seen that there is an increase in the velocity magnitude as coolant flows from inlet towards outlet. The inclusion of nanoparticles also augments the magnitude of axial velocity as seen in Fig. 5.6 which is mainly aroused from the altered thermo-physical properties of different particle volume concentration.

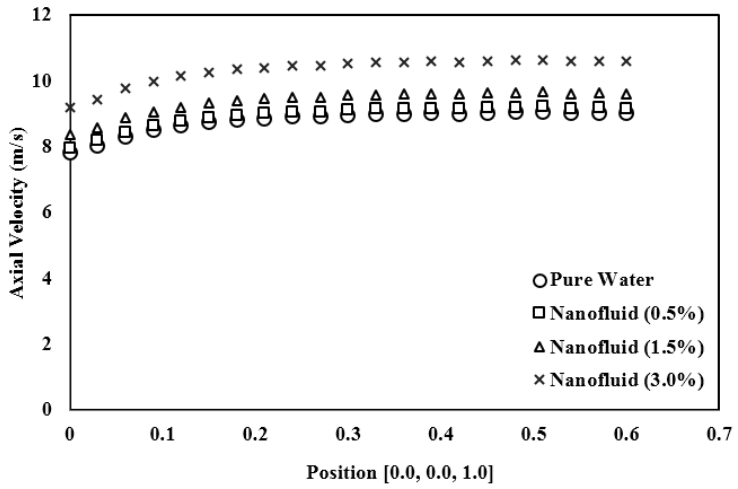

Fig. 5.6: Velocity along centerline of subchannel at *Re* = 6×10^5

5.4.3 Pressure

A plot of static pressure along the centerline of the subchannel (*P/D* =1.25) for different coolants at inlet *Re* = 6×10^5 is shown in Fig. 5.7 which depicts that there is an increase in axial pressure with the inclusion of

nanoparticles which is expected due to higher viscosity and density as the particle volume concentration is increased.

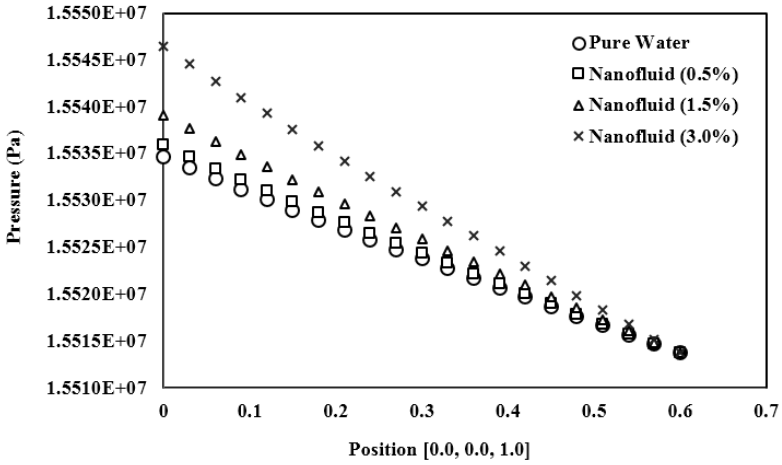

Fig. 5.7: Pressure along centerline of subchannel at $Re = 6\times10^5$

5.4.4 Turbulent Kinetic Energy

Effect on turbulent kinetic energy due to inclusion of nanoparticles at inlet $Re = 6\times10^5$ are illustrated in Fig. 5.8 which clearly dictates that turbulent kinetic energy is sharply increased by the augmentation of nanoparticle volume concentration and thus in turn heat transfer is increased too.

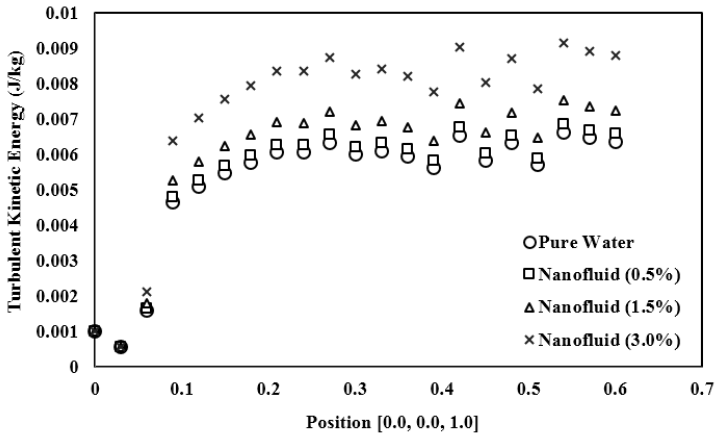

Fig. 5.8: Turbulent kinetic energy along centerline of subchannel

5.4.5 *Nu* and *h* for Constant Inlet *Re*

A convective heat transfer coefficient and Nusselt number study is carried out in Star-CCM+ for pure water and different concentrations of alumina nanofluid according to Eq. (5.4) and Eq. (5.5) respectively. Values of *Nu* are evaluated at the outlet of the subchannel to assure fully developed turbulent flow condition.

$$h = \frac{q''}{\left(T_W - T_m\right)} \tag{5.4}$$

$$Nu = \frac{h \times D_h}{k} \tag{5.5}$$

where, q'' is the constant heat flux (W/m^2), k is thermal conductivity (W/m^2.K), D_h is hydraulic diameter (m), and T_w and T_m are wall and mean bulk fluid temperature (K) respectively.

Numerical results of *Nu* and *h* for subchannel with different pitch-to-diameter (*P/D*) ratio are presented through Fig. 5.9 to 5.12 respectively and percentage of convective heat transfer increment for different nanofluid coolants are documented in Table 5.4.

From the results, it is obvious that the convective heat transfer coefficient is remarkably increased with the increment of nanoparticle volume concentration and in case of 3.0% volume concentration, convective heat transfer is increased above 22.0% compared to pure water.

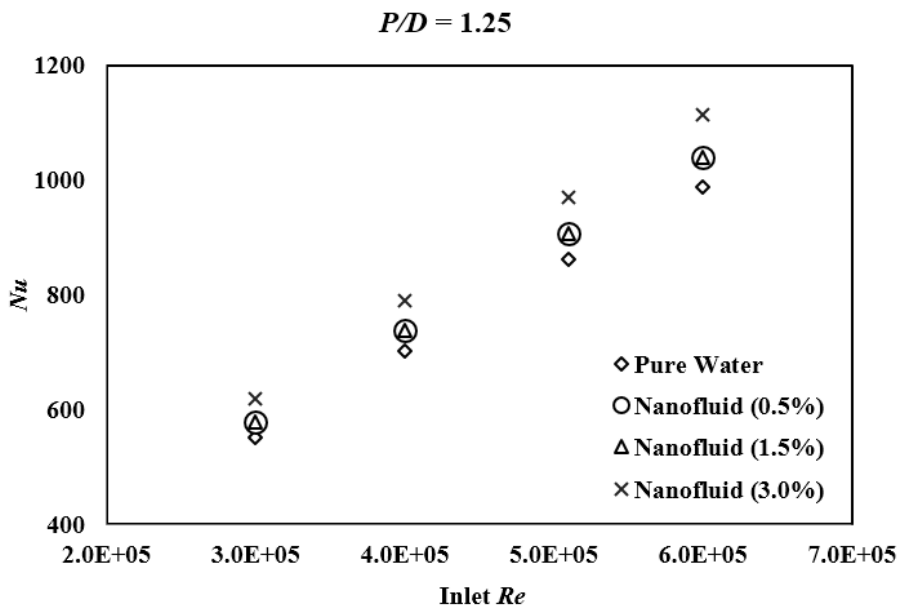

Fig. 5.9: Comparison of *Nu* for different coolants in subchannel (*P/D* 1.25)

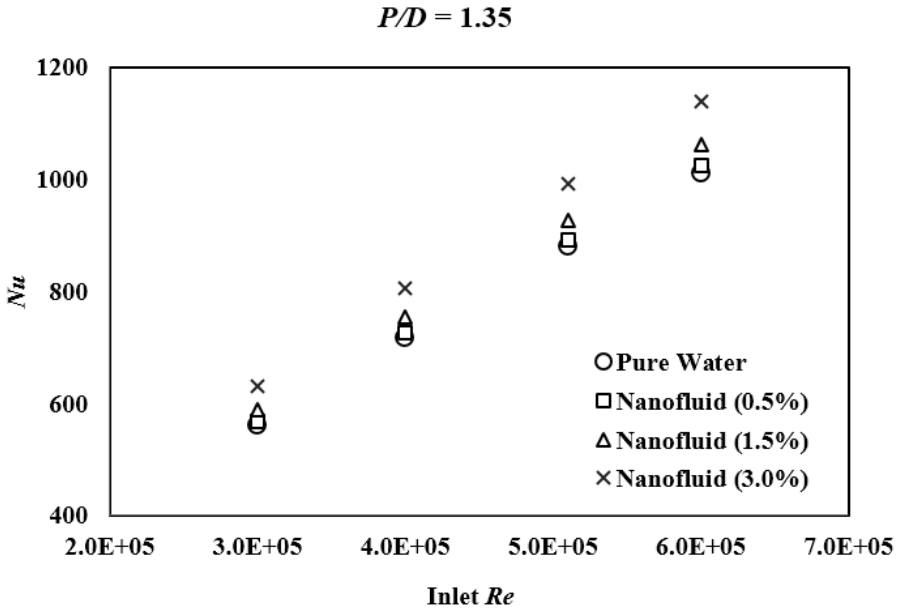

Fig. 5.10: Comparison of *Nu* for different coolants in subchannel (*P/D* 1.35)

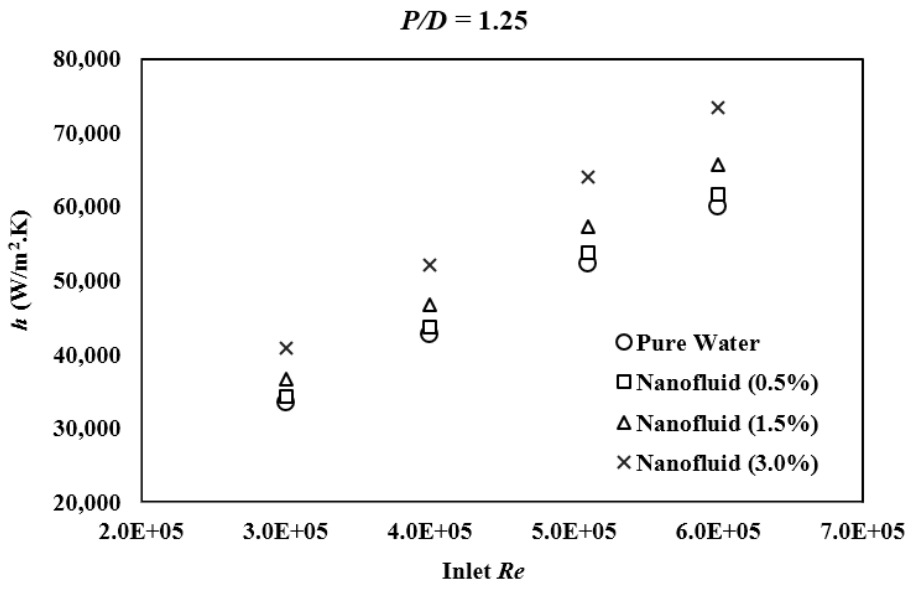

Fig. 5.11: Comparison of *h* for different coolants in subchannel (*P/D* 1.25)

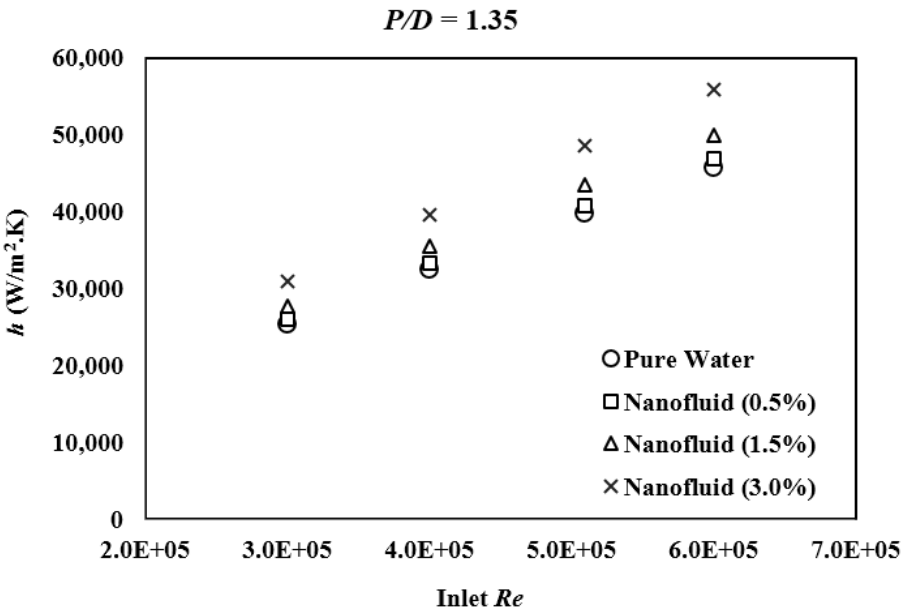

Fig. 5.12: Comparison of *h* for different coolants in subchannel (*P/D* 1.35)

Table 5.4: Heat transfer increment (%) for different nanofluid coolants

***P/D* = 1.25**

Inlet *Re*	Increment of *h* (%)		
	φ=0.5%	φ=1.5%	φ=3.0%
6×10^5	2.75	9.62	22.46
5.098×10^5	2.75	9.58	22.37
4×10^5	2.72	9.51	22.16
3×10^5	2.74	9.42	21.89

***P/D* = 1.35**

Inlet *Re*	Increment of *h* (%)		
	φ=0.5%	φ=1.5%	φ=3.0%
6×10^5	2.72	9.56	22.35
5.098×10^5	2.72	9.51	22.26
4×10^5	2.71	9.44	22.01
3×10^5	2.69	9.40	21.87

5.4.6 Comparison of Numerical Results against Correlations

In case of nanofluid with volume concentration, φ =3.0% numerical results for *Nu* are compared against two well cited correlations of Pak & Cho [3] and Maïga et al. [10] as shown in Fig. 5.13 (a) & (b) and an attempt has been made whether results of present study can be represented by either of these two correlations.

The results revealed that Pak and Cho correlation severely underestimates the numerical results for *Nu* in subchannel and deviation lies between 17 to 22 percent subject to inlet *Re* and *P/D*.

Regarding correlation of Maïga et al., it shows better approximation compared to correlation of Pak & Cho. Nevertheless, this correlation underestimates the numerical results for the range $5\times10^5 \leq Re \leq 6\times10^5$ and overestimates for $3\times10^5 \leq Re \leq 4\times10^5$ and deviations are between -0.54 to 6.66 percent depending on inlet *Re* and *P/D*.

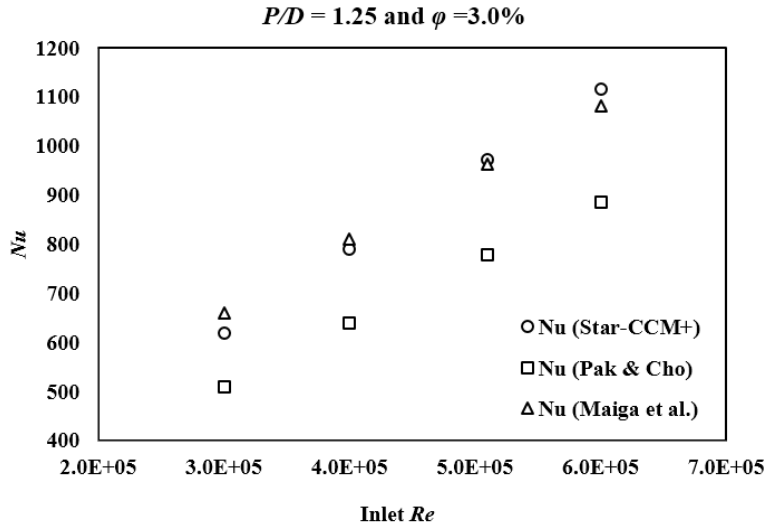

(a) *P/D* = 1.25

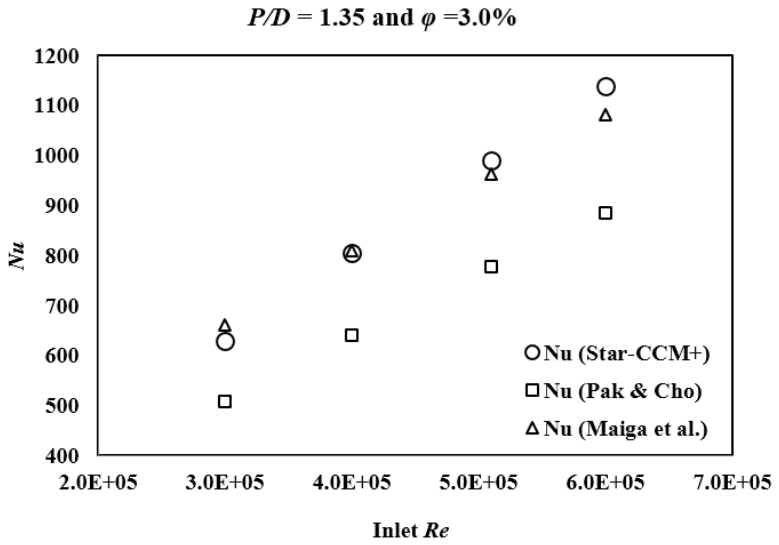

(b) *P/D* = 1.35

Fig. 5.13: Comparison of numerical *Nu* against different correlations

5.4.7 Heat Transfer Coefficient for Constant Mass Flow Rate

Another comparison of convective heat transfer coefficient, *h* with same mass flow rate at inlet boundary for φ=3.0% and *P/D* = 1.35 is carried out and results as depicted in Fig. 5.14 indicates that values of *h* for nanofluid (φ=3.0%) is somewhat lower (3.95 to 4.34 percent based on inlet mass flow rate) compared to pure water. It implies that nanofluid is capable of increasing heat transfer coefficient at the expense of more pumping power required for the existing nuclear power plants which is discussed in detail in the later part of this study.

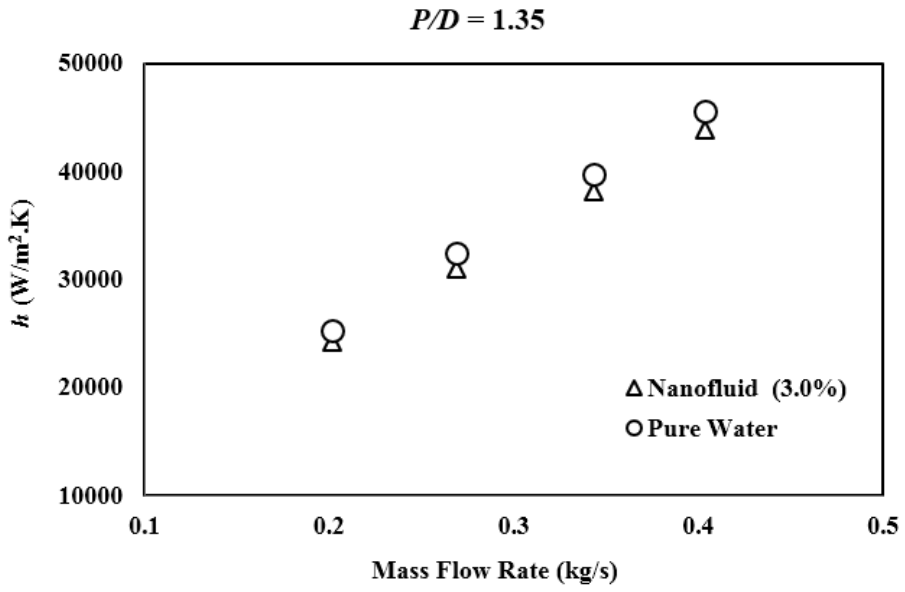

Fig. 5.14: Comparison of *h* for same mass flow rate at inlet (φ=3.0% and *P/D* = 1.35)

5.4.8 Pressure Drop

From the previous discussion, it is clear that while nanofluid enhances the convective heat transfer, the fluid itself also gets heavier compared to pure water. Hence, it is of utmost importance to determine the amount of pressure drop for the effective application of nanofluid coolant in nuclear reactors since it is directly related to the pumping power required. In this study, pressure drop along the center line of the subchannel is evaluated for different coolants and results are presented in Fig. 5.15 (a) & (b). Percentage of pressure drop increment is documented in Table 5.5.

The results shows that pressure drop is significantly increased with the augmentation of particle volume concentration and for nanofluid with φ=3.0%, pressure drop increment is about 56% higher compared to that of pure water.

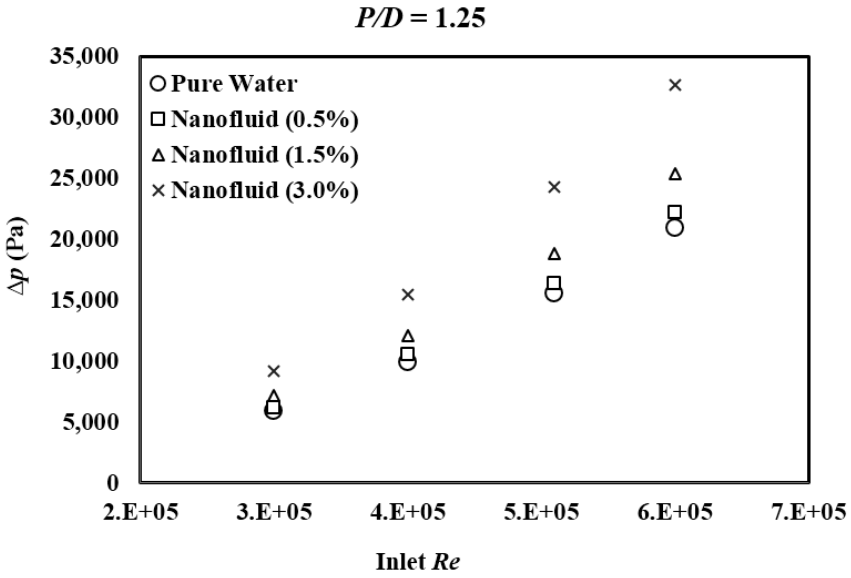

(a) *P/D* = 1.25

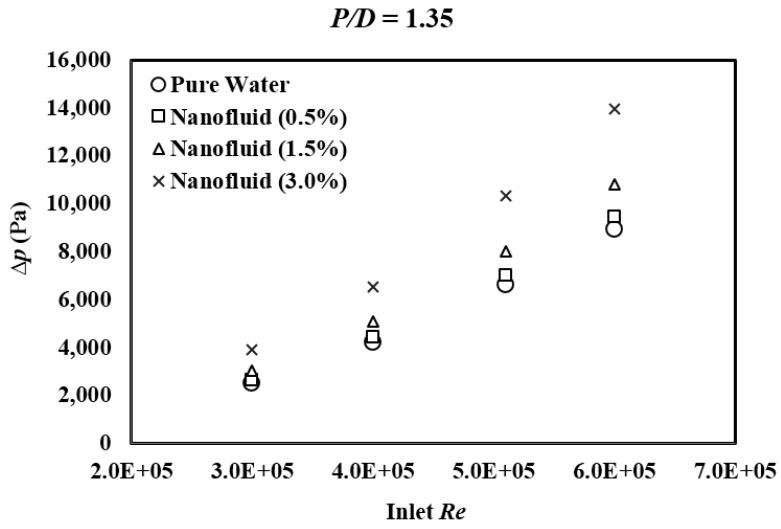

(b) *P/D* = 1.35

Fig. 5.15: Comparison of pressure drop for different coolants

Table 5.5: Pressure drop increment (%) for different nanofluid coolants

***P/D* = 1.25**

Inlet *Re*	Increment of *Δp* (%)		
	φ=0.5%	φ=1.5%	φ=3.0%
6×10^5	6.22	21.53	56.60
5.098×10^5	5.82	21.17	56.62
4×10^5	5.79	21.79	56.02
3×10^5	5.24	21.65	55.83

***P/D* = 1.35**

Inlet *Re*	Increment of *Δp* (%)		
	φ=0.5%	φ=1.5%	φ=3.0%
6×10^5	5.82	20.94	56.37
5.098×10^5	5.74	21.29	56.08
4×10^5	5.46	20.90	55.10
3×10^5	5.62	20.88	55.82

5.5 Proposed New Correction Factor

Finally, a multiple regression analysis is performed with numerical results to propose a new correction factor, β for the existing correlation of square array subchannel with pure water as suggested by Presser [60] so that *Nu* for nanofluid coolant can be approximated in such geometry. Based on regression results, β can be expressed as follows:

$$\beta = 1 + 0.0247\varphi^{1.39} \tag{5.6}$$

Nu for nanofluid can be calculated as follows:

$$Nu_{nf} = \beta * \left(Nu_{Presser} \right)_{Water} \tag{5.7}$$

The validity of above correlation is for $3\times10^5 \leq Re \leq 6\times10^5$; $0.847 \leq Pr \leq 1.011$; $1.25 \leq P/D \leq 1.35$ and $0.5\% \leq \varphi \leq 3.0\%$ in case of square array subchannel.

Conclusion

A numerical simulation has been carried out using a commercially available CFD code "Star-CCM+ (ver: 9.06.011)" to evaluate thermohydrodynamic characteristics of water/alumina (Al_2O_3) nanofluid in a square array subchannel featuring pitch-to-diameter ratio of 1.25 and 1.35 under steady state, incompressible, single phase turbulent flow condition. The homogeneous fluid assumptions with modified thermophysical properties are taken into consideration to treat water/alumina (Al_2O_3) nanofluid. Numerical results are compared against available correlations in literature and following conclusions can be conferred from the present study:

- Both convective heat transfer coefficient as well as Nusselt number are increased with increasing volume concentration of water/alumina nanofluid at constant inlet *Re*.
- The convective heat transfer increment of nanofluid is gained at the expense of larger pressure drop and hence, larger pumping power required. Despite numerical results portray that pressure drop at φ=3.0% is higher than 55%, but typical nanoparticle loading for nuclear applications is usually ≤ 0.1 vol. %. At this low concentration, nanofluid properties are almost similar to that of pure water and pressure drop is much lower but the heat transfer is increased due to higher turbulence produced near the grid spacers by the presence of nanoparticles in base fluid. One limitation of our present study is its inability to consider this phenomena of turbulence enhancement near

spacer grids for which further experimentations are required. However, from the literature [2] it is evident that with nanoparticle concentration ≤ 0.1 vol. %, it is possible to increase CHF up to 32% and uprate power density up to 20% in existing PWRs only at the expense of replacement of main coolant pumps which is considered tolerable.

- A new correction factor, β has been proposed in the following form for Presser's correlation in case of square array subchannel with pure water to predict *Nu* more effectively while nanofluid is used as coolant which is valid for $3\times10^5 \le Re \le 6\times10^5$; $0.847 \le Pr \le 1.011$; $1.25 \le P/D \le 1.35$ and $0.5\% \le \varphi \le 3.0\%$.

$$\beta = 1 + 0.0247\varphi^{1.39}$$

- Last but not least, despite analysis of reviewed literature as well as results of present study delineates that nanofluid is capable of augmenting the heat transfer capability remarkably, there is still no satisfactory explanation proposed yet regarding the prevention of clustering in nanoparticle suspensions. Therefore, while attempting to implement nanofluid coolant in PWR for long term use, clustering phenomenon of nanoparticles may eventually decrease the thermal conductivity and initiate problems like corrosion and wear inside piping and pumps. Hence, the clustering of nanoparticles to be solved first in order to utilize nanofluid as a promising coolant in PWR to achieve both extended life time of associated equipment and higher thermal efficiency.

Nomenclature

Δp	Pressure Drop	Pa
ρ	Density	kg/m^3
v	Flow Velocity	m/s
f	Friction Factor	-
L	Length of Flow Channel	m
l_e	Entrance Length	m
EI	Entrance Length Number	-
D_h	Hydraulic Diameter	m
μ	Dynamic Viscosity	$N.s/m^2$
Re	Reynolds Number	-
Nu	Nusselt Number	-
Pr	Prandtl Number	-
Pe	Peclet Number	-
h	Convective Heat Transfer Coefficient	$W/m^2.K$
k	Thermal Conductivity	W/m.K
C_p	Specific Heat	J/kg.K
T_m	Bulk Temperature of Fluid	K
T_w	Surface Temperature of Heater Rod	K
P	Rod Pitch	m

D	Rod Diameter	m
Q	Total Heat Input	W
q''	Heat Flux	W/m^2
$\dot{m}$	Mass Flow Rate	kg/sec
φ	Volume Concentration of Nanoparticles	%

Subscript

$_{nf}$	Nanofluid
$_{bf}$	Basefluid
$_{P}$	Particle

References

1. Buongiorno, J., et al., *Nanofluids for enhanced economics and safety of nuclear reactors: an evaluation of the potential features, issues, and research gaps.* Nuclear Technology, 2008. **162**(1): p. 80-91.
2. Buongiorno, J. and L.-w. Hu, *Nanofluids for Enhanced Economics and Safety of Nuclear Reactors* 2007: University Park Hotel at MIT, Cambridge, MA.
3. Pak, B.C. and Y.I. Cho, *Hydrodynamic and heat transfer study of dispersed fluids with submicron metallic oxide particles.* Experimental Heat Transfer an International Journal, 1998. **11**(2): p. 151-170.
4. Xuan, Y. and Q. Li, *Investigation on convective heat transfer and flow features of nanofluids.* Journal of Heat transfer, 2003. **125**(1): p. 151-155.
5. Anoop, K.B., T. Sundararajan, and S.K. Das, *Effect of particle size on the convective heat transfer in nanofluid in the developing region.* International Journal of Heat and Mass Transfer, 2009. **52**(9–10): p. 2189-2195.
6. Chandrasekar, M., S. Suresh, and A. Chandra Bose, *Experimental studies on heat transfer and friction factor characteristics of Al_2O_3/water nanofluid in a circular pipe under laminar flow with wire coil inserts.* Experimental Thermal and Fluid Science, 2010. **34**(2): p. 122-130.

7. Suresh, S., M. Chandrasekar, and S. Chandra Sekhar, *Experimental studies on heat transfer and friction factor characteristics of CuO/water nanofluid under turbulent flow in a helically dimpled tube.* Experimental Thermal and Fluid Science, 2011. **35**(3): p. 542-549.

8. Hojjat, M., et al., *Turbulent forced convection heat transfer of non-Newtonian nanofluids.* Experimental Thermal and Fluid Science, 2011. **35**(7): p. 1351-1356.

9. Maïga, S.E.B., et al., *Heat transfer enhancement by using nanofluids in forced convection flows.* International Journal of Heat and Fluid Flow, 2005. **26**(4): p. 530-546.

10. El Bécaye Maïga, S., et al., *Heat transfer enhancement in turbulent tube flow using Al_2O_3 nanoparticle suspension.* International Journal of Numerical Methods for Heat & Fluid Flow, 2006. **16**(3): p. 275-292.

11. Bianco, V., et al., *Numerical investigation of nanofluids forced convection in circular tubes.* Applied Thermal Engineering, 2009. **29**(17–18): p. 3632-3642.

12. Wang, X.-Q. and A.S. Mujumdar, *A review on nanofluids-part I: theoretical and numerical investigations.* Brazilian Journal of Chemical Engineering, 2008. **25**(4): p. 613-630.

13. Conner, M.E., E. Baglietto, and A.M. Elmahdi, *CFD methodology and validation for single-phase flow in PWR fuel assemblies.* Nuclear Engineering and Design, 2010. **240**(9): p. 2088-2095.

14. Liu, C.C. and Y.M. Ferng, *Numerically simulating the thermal–hydraulic characteristics within the fuel rod bundle using CFD*

methodology. Nuclear Engineering and Design, 2010. **240**(10): p. 3078-3086.

15. Palandi, S.J., M. Rahimi-Esbo, and Y. Vazifeshenas, *Comparison of thermo-hydraulic performance of nanofluids and mixing vanes in a triangular fuel rod bundle.* Journal of the Brazilian Society of Mechanical Sciences and Engineering, 2015. **37**(1): p. 173-186.
16. Wu, X. and A.C. Trupp, *Experimental study on the unusual turbulence intensity distributions in rod-to-wall gap regions.* Experimental Thermal and Fluid Science, 1993. **6**(4): p. 360-370.
17. Masuda, H., A. Ebata, and K. Teramae, *Alteration of thermal conductivity and viscosity of liquid by dispersing ultra-fine particles. Dispersion of Al_2O_3, SiO_2 and TiO_2 ultra-fine particles.* 1993.
18. Lee, S., et al., *Measuring thermal conductivity of fluids containing oxide nanoparticles.* Journal of Heat Transfer, 1999. **121**(2): p. 280-289.
19. Wang, X., X. Xu, and S.U. S. Choi, *Thermal conductivity of nanoparticle-fluid mixture.* Journal of thermophysics and heat transfer, 1999. **13**(4): p. 474-480.
20. Murshed, S., K. Leong, and C. Yang, *Enhanced thermal conductivity of TiO_2—water based nanofluids.* International Journal of Thermal Sciences, 2005. **44**(4): p. 367-373.
21. Maxwell, J.C., *A treatise on electricity and magnetism.* Vol. 1. 1881: Clarendon press.

22. Xie, H., et al., *Dependence of the thermal conductivity of nanoparticle-fluid mixture on the base fluid.* Journal of Materials Science Letters, 2002. **21**(19): p. 1469-1471.

23. Chopkar, M., et al., *Effect of particle size on thermal conductivity of nanofluid.* Metallurgical and Materials Transactions A, 2008. **39**(7): p. 1535-1542.

24. Eastman, J., et al., *Anomalously increased effective thermal conductivities of ethylene glycol-based nanofluids containing copper nanoparticles.* Applied physics letters, 2001. **78**(6): p. 718-720.

25. Hamilton, R. and O. Crosser, *Thermal conductivity of heterogeneous two-component systems.* Industrial & Engineering chemistry fundamentals, 1962. **1**(3): p. 187-191.

26. Beck, M.P., et al., *The effect of particle size on the thermal conductivity of alumina nanofluids.* Journal of Nanoparticle Research, 2009. **11**(5): p. 1129-1136.

27. Li, C.H., et al., *Transient and steady-state experimental comparison study of effective thermal conductivity of Al_2O_3/ water nanofluids.* Journal of Heat Transfer, 2008. **130**(4): p. 042407.

28. Das, S.K., et al., *Temperature dependence of thermal conductivity enhancement for nanofluids.* Journal of Heat Transfer, 2003. **125**(4): p. 567-574.

29. Bhattacharya, P., et al., *Brownian dynamics simulation to determine the effective thermal conductivity of nanofluids.* Journal of Applied Physics, 2004. **95**(11): p. 6492-6494.

30. Prasher, R., P. Bhattacharya, and P.E. Phelan, *Thermal conductivity of nanoscale colloidal solutions (nanofluids).* Physical Review Letters, 2005. **94**(2): p. 025901.

31. Li, C. and G. Peterson, *Mixing effect on the enhancement of the effective thermal conductivity of nanoparticle suspensions (nanofluids).* International Journal of Heat and Mass Transfer, 2007. **50**(23): p. 4668-4677.

32. Jang, S.P. and S.U. Choi, *Role of Brownian motion in the enhanced thermal conductivity of nanofluids.* Applied physics letters, 2004. **84**(21): p. 4316-4318.

33. Keblinski, P., J.A. Eastman, and D.G. Cahill, *Nanofluids for thermal transport.* Materials today, 2005. **8**(6): p. 36-44.

34. Evans, W., J. Fish, and P. Keblinski, *Role of Brownian motion hydrodynamics on nanofluid thermal conductivity.* Applied Physics Letters, 2006. **88**(9): p. 093116.

35. Evans, W., et al., *Effect of aggregation and interfacial thermal resistance on thermal conductivity of nanocomposites and colloidal nanofluids.* International Journal of Heat and Mass Transfer, 2008. **51**(5): p. 1431-1438.

36. Keblinski, P., R. Prasher, and J. Eapen, *Thermal conductance of nanofluids: is the controversy over?* Journal of Nanoparticle research, 2008. **10**(7): p. 1089-1097.

37. Feng, Y., et al., *The effective thermal conductivity of nanofluids based on the nanolayer and the aggregation of nanoparticles.* Journal of Physics D: Applied Physics, 2007. **40**(10): p. 3164.

38. Prasher, R., P.E. Phelan, and P. Bhattacharya, *Effect of aggregation kinetics on the thermal conductivity of nanoscale colloidal solutions (nanofluid).* Nano Letters, 2006. **6**(7): p. 1529-1534.

39. Yu, C.-J., et al., *Observation of molecular layering in thin liquid films using X-ray reflectivity.* Physical Review Letters, 1999. **82**(11): p. 2326.

40. Yu, W. and S. Choi, *The role of interfacial layers in the enhanced thermal conductivity of nanofluids: a renovated Maxwell model.* Journal of Nanoparticle Research, 2003. **5**(1-2): p. 167-171.

41. Ozerinc, S., *Heat transfer enhancement with nanofluids.* Mémoire de maıtrise, 2010.

42. Keblinski, P., et al., *Mechanisms of heat flow in suspensions of nano-sized particles (nanofluids).* International journal of heat and mass transfer, 2002. **45**(4): p. 855-863.

43. Domingues, G., et al., *Heat transfer between two nanoparticles through near field interaction.* Physical review letters, 2005. **94**(8): p. 085901.

44. Ahn, H.S., et al., *Experimental study of critical heat flux enhancement during forced convective flow boiling of nanofluid on a short heated surface.* International Journal of Multiphase Flow, 2010. **36**(5): p. 375-384.

45. Kim, S.J., et al., *Subcooled flow boiling heat transfer of dilute alumina, zinc oxide, and diamond nanofluids at atmospheric pressure.* Nuclear Engineering and Design, 2010. **240**(5): p. 1186-1194.

46. Versteeg, H.K. and W. Malalasekera, *An introduction to computational fluid dynamics: the finite volume method*. 2007: Pearson Education.

47. Johannessen, S.R., *Use of CFD to Study Hydrodynamic Loads on Free-Fall Lifeboats in the Impact Phase.: A verification and validation study.* 2012.

48. *STAR-CCM+ Training Manual, Version 05/14, CD-Adapco.*

49. Maïga, S., et al. *Heat transfer enhancement in forced convection laminar tube flow by using nanofluids.* in *Proc Int Symp Adv Comput Heat Transf CHT04, April 19-24; Norway*. 2004.

50. Brinkman, H., *The viscosity of concentrated suspensions and solutions.* The Journal of Chemical Physics, 1952. **20**(4): p. 571-571.

51. Batchelor, G., *The effect of Brownian motion on the bulk stress in a suspension of spherical particles.* Journal of Fluid Mechanics, 1977. **83**(01): p. 97-117.

52. Maïga, S.E.B., et al., *Heat transfer behaviours of nanofluids in a uniformly heated tube.* Superlattices and Microstructures, 2004. **35**(3): p. 543-557.

53. Yadigaroglu, G., et al., *Trends and needs in experimentation and numerical simulation for LWR safety.* Nuclear Engineering and Design, 2003. **221**(1): p. 205-223.

54. Házi, G., *On turbulence models for rod bundle flow computations.* Annals of Nuclear Energy, 2005. **32**(7): p. 755-761.

55. Lee, C. and Y. Choi, *Comparison of thermo-hydraulic performances of large scale vortex flow (LSVF) and small scale vortex flow (SSVF) mixing vanes in 17× 17 nuclear rod bundle.* Nuclear Engineering and Design, 2007. **237**(24): p. 2322-2331.

56. Yakhot, V., et al., *Development of turbulence models for shear flows by a double expansion technique.* Physics of Fluids A: Fluid Dynamics (1989-1993), 1992. **4**(7): p. 1510-1520.

57. Smith III, L., et al., *Benchmarking computational fluid dynamics for application to PWR fuel.* Proceedings of ICONE, 2002. **10**.

58. Shih, T.-H., et al., *A new k-epsilon eddy viscosity model for high Reynolds number turbulent flows: Model development and validation.* 1994.

59. *Introduction to ANSYS FLUENT: Customer Training Material, Release 13, December 2010.* .

60. Presser, K.H., *Wärmeübergang und Druckverlust an Reaktorbrennelementen in Form längsdurchströmter Rundstabbündel.* 1967, Kernforschungsanlage, Zentralbibliothek.

61. Xuan, Y. and W. Roetzel, *Conceptions for heat transfer correlation of nanofluids.* International Journal of heat and Mass transfer, 2000. **43**(19): p. 3701-3707.